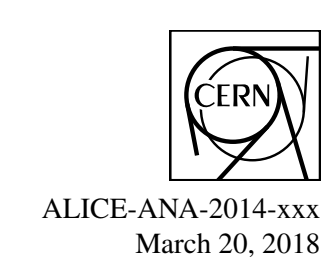
# EUROPEAN ORGANIZATION FOR NUCLEAR RESEARCH





Production of pions, kaons and protons in p-Pb collisions at  $\sqrt{s_{NN}}$  =8.16 TeV

Pavel Larionov<sup>1</sup>, Paula Matuoka<sup>1,3</sup>, Silvia Pisano<sup>1,2</sup>, Marco Toppi<sup>1</sup>

Laboratori Nazionali di Frascati - INFN, Frascati, Italy
 *Via Enrico Fermi, 40, 00044 Frascati (Rome, Italy)* Museo Storico della Fisica e Centro Studi e Ricerche Enrico Fermi
 *Piazza del Viminale 1 00184 Roma (Italy)* Instituto de Física da Universidade de São Paulo
 *Rua do Matão, Tr.R, 187, 05508-090, São Paulo (Brazil)*

Email: silvia.pisano@lnf.infn.it

#### **Abstract**

At the end of 2016 the ALICE detector, installed at the LHC, collected p-Pb data at a center of mass energy equal to  $\sqrt{s_{\rm NN}}=8.16$  TeV. These data represent an important chance to test the emergence of possible initial state effects, by comparing the spectra of identified light hadrons extracted in this dataset to the ones measured in previous pp and Pb-Pb data in a wide transverse momentum range. In this analysis, the first results on transverse momentum spectra for identified  $\pi$ , K and p at  $\sqrt{s_{\rm NN}}=8.16$  TeV measured through the capabilities of the ALICE ITS, TPC and TOF systems are presented. This analysis has been performed at midrapidity over a wide transverse-momenta range (100 MeV/ $c < p_{\rm T} < 20$  GeV/c) for different multiplicity classes ranging from central to peripheral ones.

# Contents

1	Ana	Analysis summary				
	1.1	Included detectors	3			
	1.2	Useful Twiki pages	3			
	1.3	Git repository for preliminary results	3			
	1.4	List fo relevant presentations	3			
2	Con	nmon data sets, event selection and binning	4			
3	ITS	sa	6			
	3.1	Track selection	6			
	3.2	Particle identification	6			
	3.3	Raw spectra	8			
	3.4	Corrections	8			
		3.4.1 Efficiency correction	8			
		3.4.2 Primary corrections	12			
	3.5	Systematic uncertainties	15			
4 TPC						
	4.1	Track selection	17			
	4.2	TPC-based yield extraction in the low- $p_T$ part: fit to $N_{\sigma}$	17			
	4.3 Raw spectra					
4.4 Particle ratios						
	4.5	Corrections	19			
		4.5.1 Efficiency correction	19			
		4.5.2 Geant/Fluka correction	31			
		4.5.3 Geant3/Geant4 correction	31			
		4.5.4 Primary fraction corrections	31			
	4.6	Systematics	37			
		4.6.1 Systematics on event and track selection cuts	37			

		4.6.2 Yield extraction	37
5	TOF		48
	5.1	TOF track requirements	48
	5.2	PID with TOF detector and signal extraction	48
	5.3	Primary fraction	52
	5.4	Efficiency correction	58
6	Com	bined Results	65

# 1 Analysis summary

The analysis is based on the p-Pb data collected in 2016 at a center of mass energy of 8.16 TeV. The data set considered in the analysis is LHC16r, to which the Monte Carlo production LHC17f3a\_cent\_fix is anchored.

The following runs have been considered:

266318, 266317, 266316, 266208, 266197, 266196, 266187, 265754, 265744, 265607, 265596, 265594

## 1.1 Included detectors

The analysis has been performed based on the information from the following detectors:

- ITSsa

Analyzer: Pavel Larionov

- TPC

Analyzer: Silvia Pisano

TOF

Analyzer: Marco Toppi

Add the subrange of the different analysis

## 1.2 Useful Twiki pages

To be filled

## 1.3 Git repository for preliminary results

To be filled

## 1.4 List fo relevant presentations

Presentations with details on the ongoing analyses in the different Spectra-PAG or Light-Flavors PWG meetings, as well as talks given at the ALICE Physics Week, can be found at the following links:

- PWG-LF QM Preview Session (March 5<sup>th</sup>, 2018): https://indico.cern.ch/event/708109/
- Spectra-PAG Meeting (February 26<sup>th</sup>, 2018): https://indico.cern.ch/event/708519/

- Spectra-PAG Meeting (January 29<sup>th</sup>, 2018): https://indico.cern.ch/event/700770
- Spectra-PAG Meeting (November 27<sup>th</sup>, 2018): https://indico.cern.ch/event/684087
- Spectra-PAG Meeting (November 27<sup>th</sup>, 2018): https://indico.cern.ch/event/684087
- ALICE Physics Week Laboratori Nazionali di Frascati (February 5<sup>th</sup>, 2018): https://indico.cern.ch/event/687851/

# 2 Common data sets, event selection and binning

The data set considered in the analysis is LHC16r, to which the Monte Carlo production LHC17f3a\_cent\_fix is anchored. A common event selection has been adopted for the three analysis, *i.e.* the one implemented in the cut

AliEventCuts fEventCuts

It includes the following selections:

## **Pre-trigger selections**

## **Trigger selection**

Minimum Bias (MB) p-Pb events are selected through AliVEvent::kINT7.

## **Multiplicity selection**

Multiplicity of an event is estimated through VOM as

```
fMultSelection = (AliMultSelection*) fESD->FindListObject("MultSelection");
    percentile = fMultSelection -> GetMultiplicityPercentile("VOM");
```

The following multiplicity binning is adopted throughout the three analyses:

```
[0-5]% [5-10]% [10-20]% [20-30]% [30-40]% [40-50]% [50-60]% [60-80]% [80-100]%
```

#### Vertex selection

Vertexes are reconstructed through the aid of ITS and TPC information. Track vertex is adopted as default; if the latter is not available, the one from SPD is considered. In order for an event to

be selected vertex coordinate have to satisfy the following condition:

$$|Z_{vertex}| < 10 cm \tag{1}$$

In the software, abovementioned requests are implemented through:

fEventCuts.PassedCut(AliEventCuts::kVertexQuality)
fEventCuts.PassedCut(AliEventCuts::kVertexPosition)
included in the fEventCuts.AcceptEvent(fESD) method.

### 3 ITSsa

#### 3.1 Track selection

The track selection for each accepted event was based on ITS pure standalone tracks<sup>1</sup> together with ITS refit requirement. The following standard ITS standalone tracks cuts have been applied:

- 1. Pseudo-rapidity and rapidity selection:  $|\eta| < 0.8 + 0 < y_{CMS} < 0.5$ ;
- 2. The required number of ITS clusters: at least one cluster in SPD ( $N_{cls}^{SPD} \geq 1$ ), at least three clusters in SDD+SSD ( $N_{cls}^{SDD+SSD} \geq 3$ );
- 3.  $\chi^2/N_{cls}$  < 2.5: in order to remove the contamination from fake tracks;
- 4. Cut on the Distance of Closest Approach (DCA) in Z plane: the maximum distance (in  $\mu$ m is set to  $7\sigma$ ;
- 5. Cut on the transverse distance of closest approach DCA<sub>xy</sub>  $< 7\sigma$ ; The DCA cuts are applied in order to remove the contamination from secondary tracks.

After the track cuts were applied, the tracking efficiency was evaluated using the Monte Carlo runs from LHC17f3a\_cent\_fix (EPOS MC generator) for the corresponding multiplicity classes. Figure 1a shows the tracking efficiency for particle species in integrated multiplicity. Figure 1b depicts the comparison of the tracking efficiency for low and high multiplicity classes. In Figure 1c the tracking efficiency of  $K^+$  is shown as an example for all multiplicity classes including the minimum bias case (MB).

#### 3.2 Particle identification

The particle identification (PID) is based on the energy loss information provided by four outer layers of the ITS: two layers of silicon drift detectors and two layers of silicon strip detectors. As the energy loss distribution in silicon layers of the ITS is a Landau distribution with a typical long tail, a truncated mean approach has been chosen in order to reduce the energy loss fluctuations. The method implies the assignment of the average of two lowest dE/dx points in case if four points were measured or a weighted sum of the lowest and the second lowest points in case of 3 measured dE/dx values as a dE/dx signal of a track. This is done by calling the GetITSSignal method for each track. Figure 2 depicts the obtained truncated mean energy loss distribution after applying the track cuts. Here, the black curves represent the hybrid Bethe-Bloch parametrization. The particle identification method in this analysis uses the truncated mean energy loss distribution to assign a track to a particle specie depending on the distance from the expected BB parametrization<sup>2</sup>, track-by-track.

<sup>&</sup>lt;sup>1</sup>Tracks reconstructed with the ITS stand-alone tracking algorithm, where only the ITS clusters are used for track reconstruction.

<sup>&</sup>lt;sup>2</sup>So-called Truncated Mean cut.

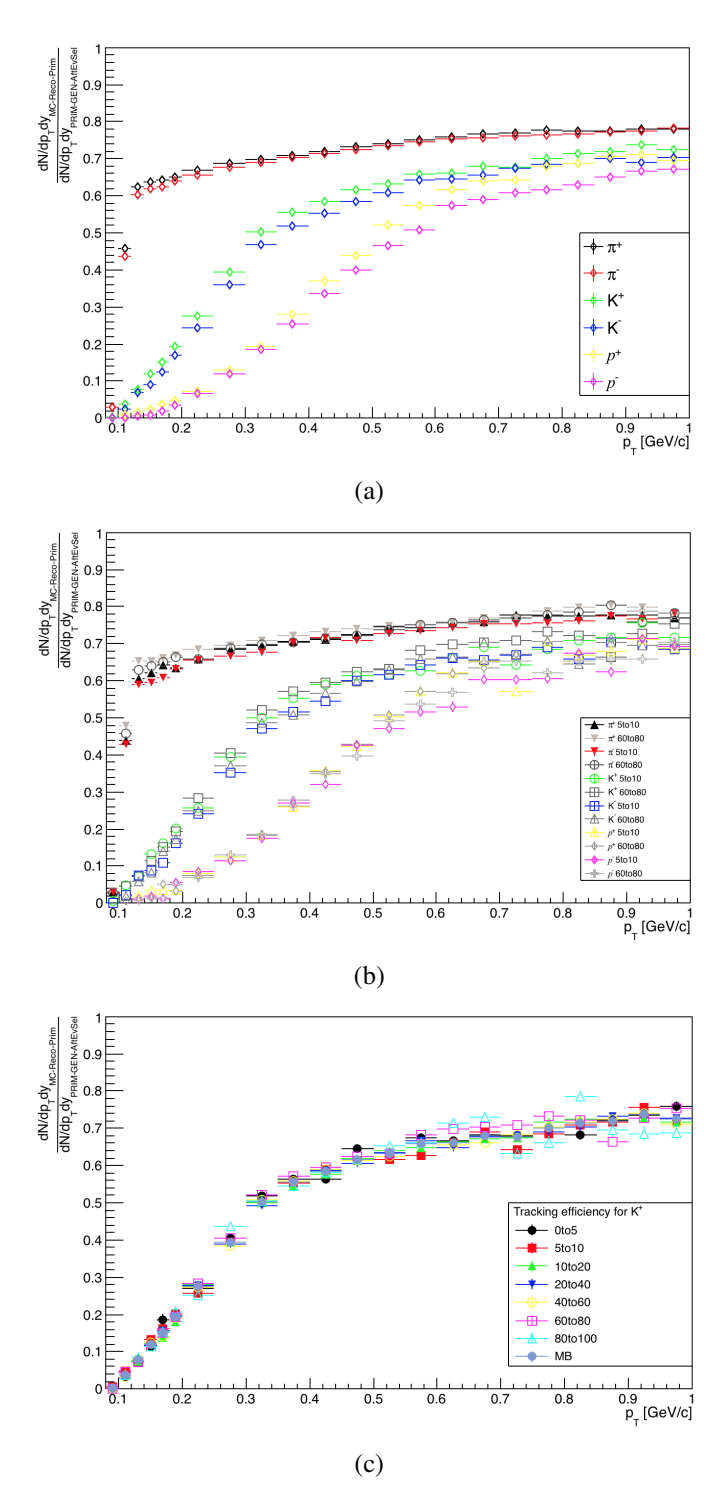


Fig. 1: Tracking efficiency for: (a) all particle species in integrated multiplicity, (b) all particle species in low and high multiplicity classes, (c)  $K^+$  in all multiplicity classes including the MB.

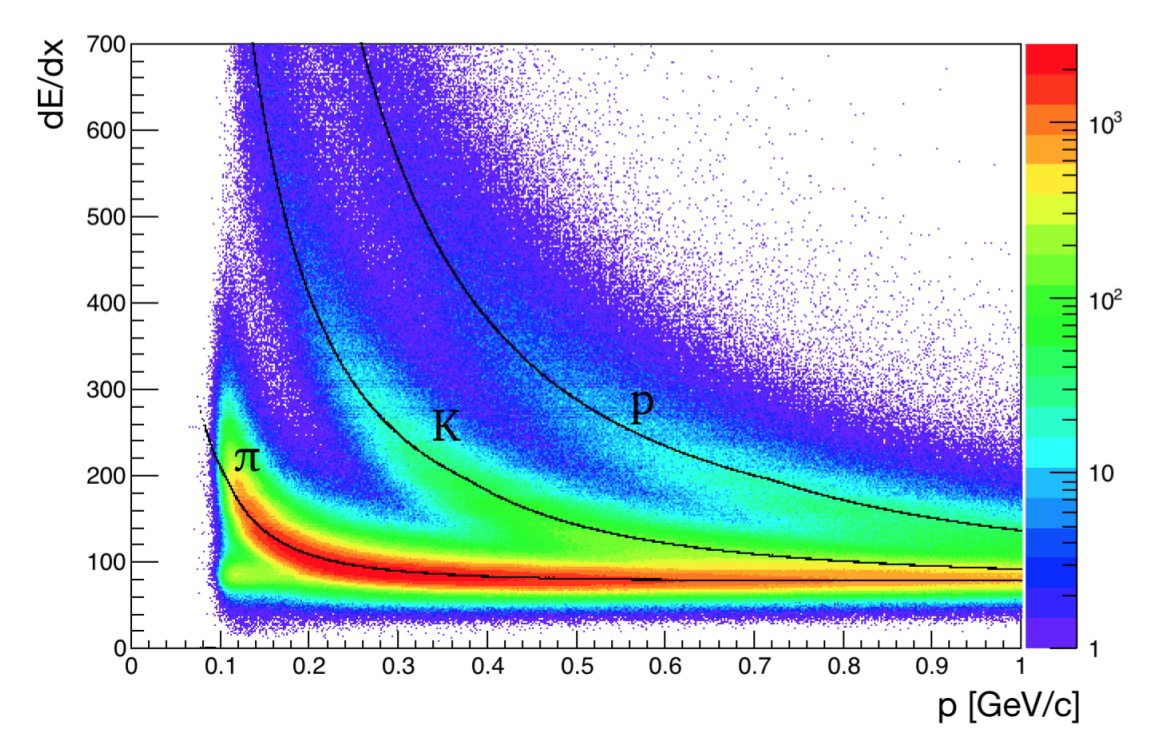


Fig. 2: Energy loss distribution in the ITS layers, obtained with the truncated mean approach.

## 3.3 Raw spectra

The raw spectra was extracted using the truncated mean PID method. The spectra are divided by the bin width and the bin of rapidity for better representation and comparison.

### 3.4 Corrections

The raw spectra has to be corrected in order to take into account the inefficiency of the detector, production of secondary particles and inefficiency of the MC generator in production of certain particle species.

### 3.4.1 Efficiency correction

The inefficiency of the detector performance, i.e., presence of dead or not-working channels as well as inefficiency in track reconstruction, changes the reconstructed spectra. The correction factor which takes into account the underlined is obtained from the Monte Carlo simulation:

$$C_{i} = \frac{dN/dp_{T}dy_{MC,RAW}}{dN/dp_{T}dy_{Prim-Gen-AftEvSel}}$$
(2)

The efficiency correction factor is calculated for each multiplicity class (Fig. 4b shows an example for  $\pi^+$ ). Then, the raw spectra is divided by the latter (Figure 5).

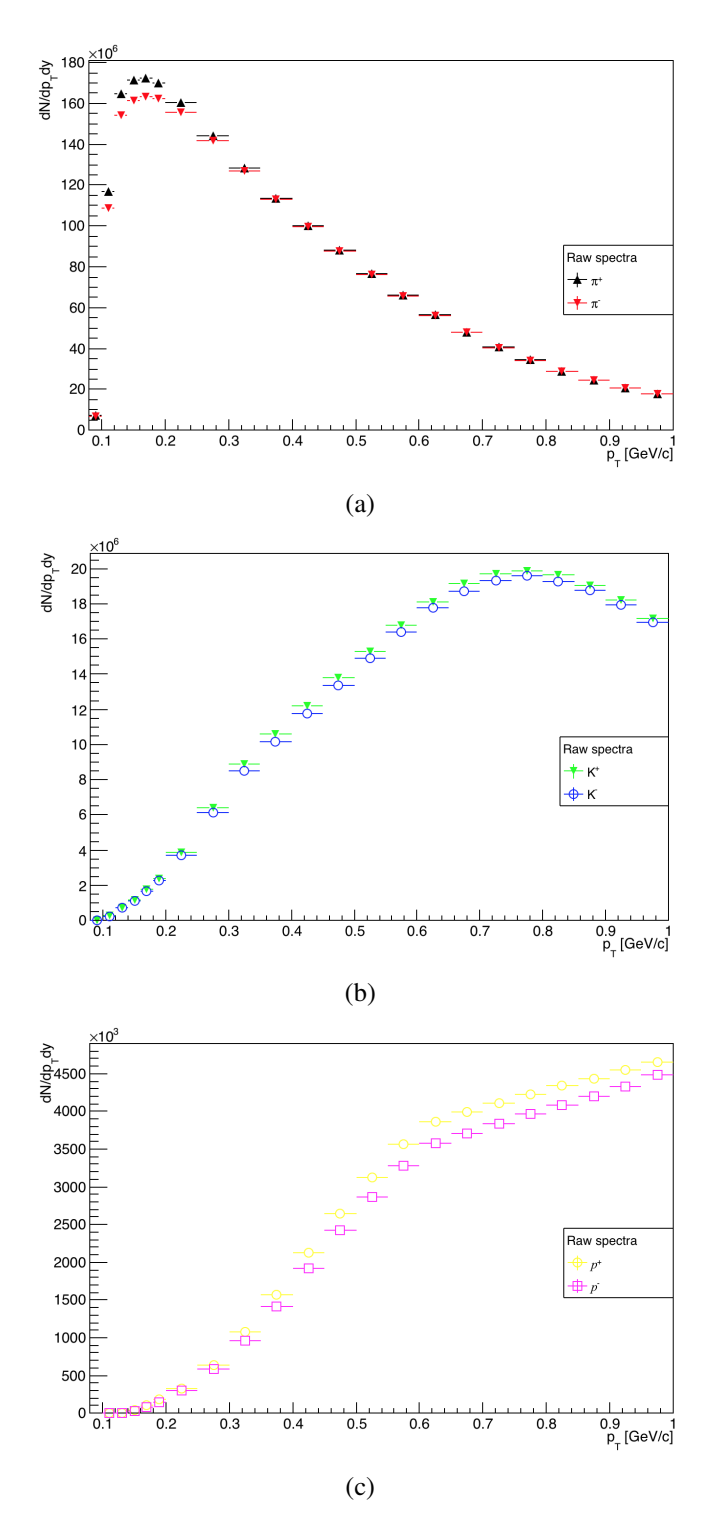


Fig. 3: Raw spectra for: (a) pions (b) kaons (c) protons

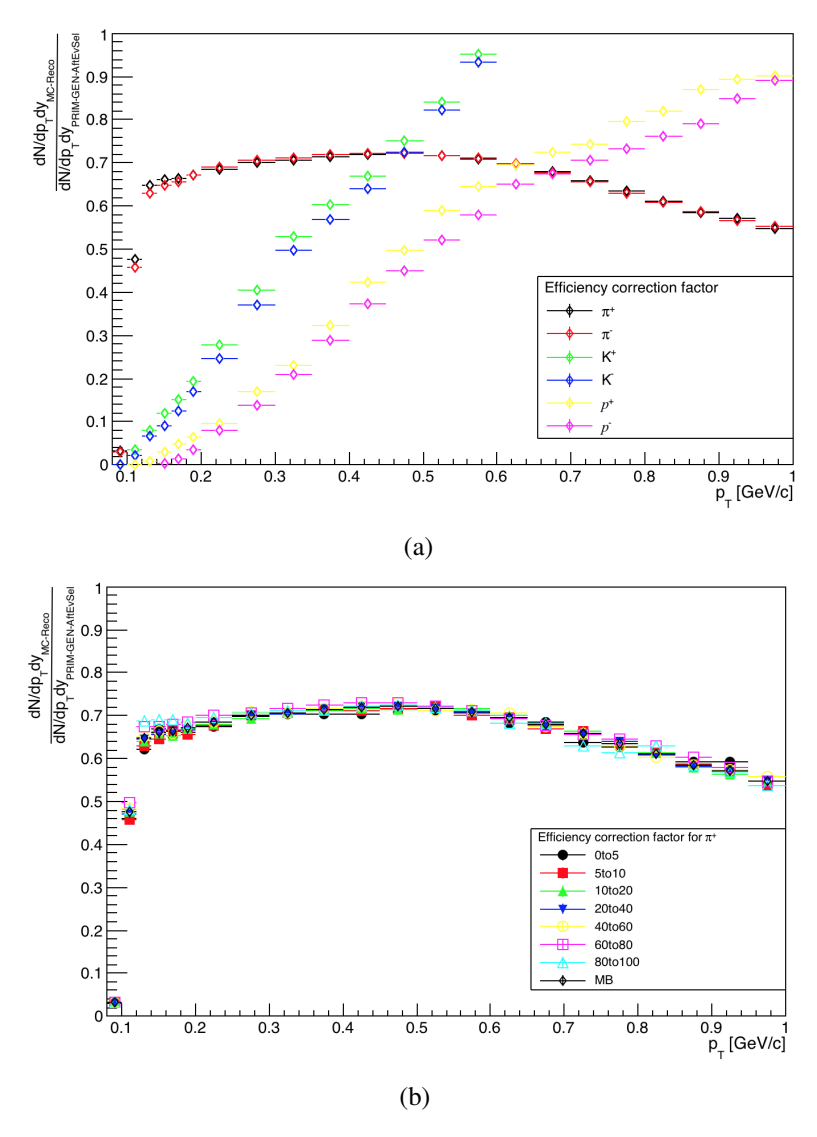


Fig. 4: Efficiency correction factor for: (a) all species in integrated multiplicity , (b)  $\pi^+$  in all multiplicity classes including MB.

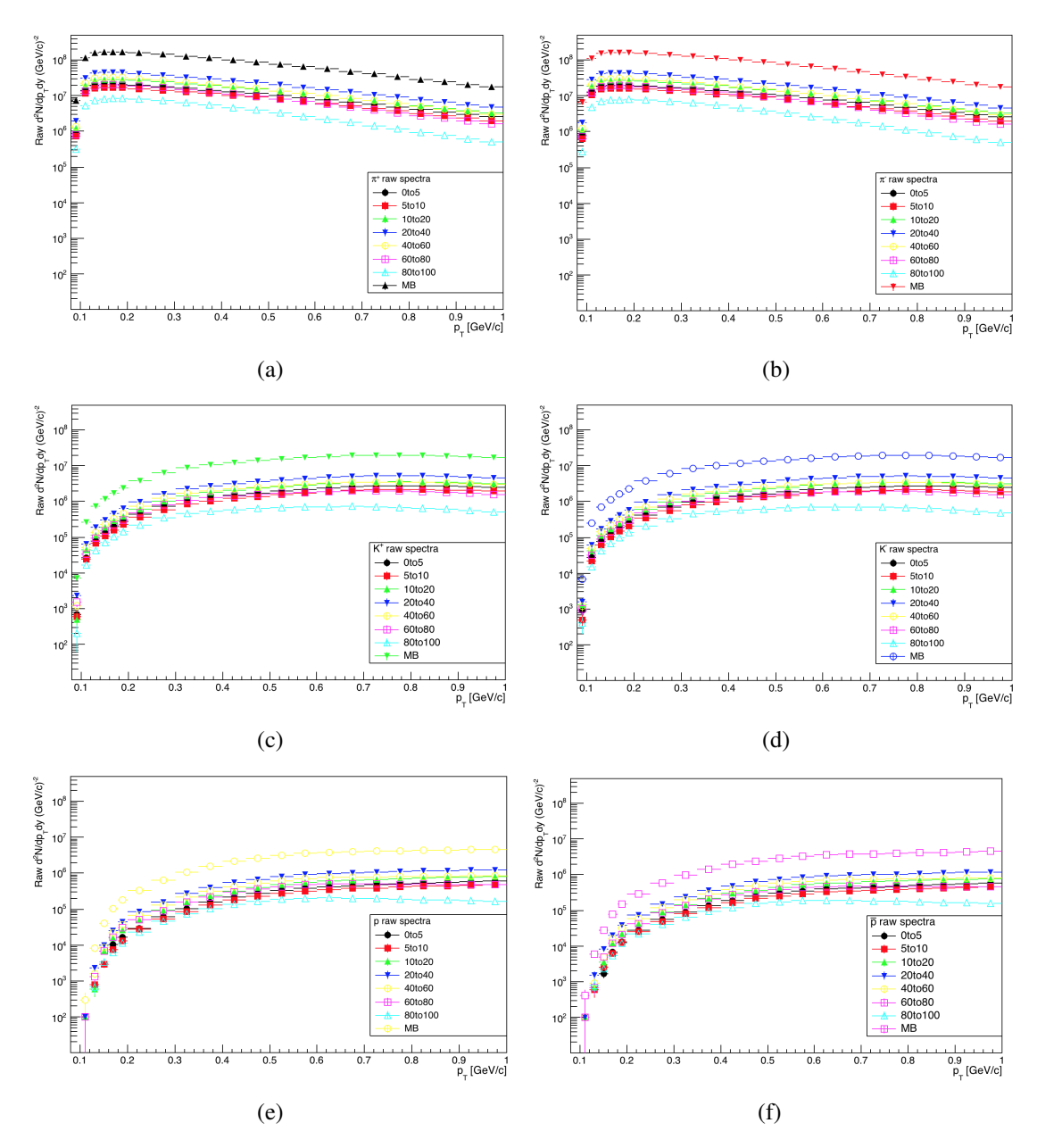


Fig. 5: Raw spectra in all multiplicity classes including MB for: (a)  $\pi^+$  (b)  $\pi^-$  (c)  $K^+$  (d)  $K^-$  (e) p (f)  $\bar{p}$ .

## 3.4.2 Primary corrections

In order to obtain the final spectra of primary particles, the contribution from secondaries coming from the decay of strange baryons or from detector material have to be subtracted. Primary particles are the one directly produced in the collisions, or produced by strong mechanisms. The fraction of primary composing the final yield is estimated by looking at the distribution of the Distance of closest approach in the xy plane ( $DCA_{xy}$ ). Templates for the  $DCA_{xy}$  distribution of the secondaries are produced through the Monte Carlo truth information. In particular, the contributions modeled on MC are:

 primary particles: templates are produced by using the MC information of the class AliStack:

that identify final particles produced directly in the collisions.

2. **secondary from weak decays**. Strange baryons can decay through weak interaction as, e.g.,  $\Lambda \to \pi p$ , leading to a contamination in the final spectra for protons and pions. Similarly to the previous case, the information is got through the method

3. **secondary material**: in the case of (positive) protons, further contamination can appear due to the proton production on detector material. It is identified through the method

These contributions are subtracted for pions and protons, the latter (secondary from material) being considered for positive protons only, since it is negligible for other species. As to data, a "pure" sample of particle of the desired identity is produced by applying a cut on  $N_{\sigma}$  ( $N_{\sigma} < 2$ ). The MC distributions are scaled to data, that are then expressed as a linear combination of the former. The fractions of the different contributions are fitted and the primary fraction are extracted for  $p_T$  and multiplicity bins. Only for the positive proton case, due to the lack of events for the template describing the secondary from materials, the primary fraction is estimated integrated in multiplicity. The final fraction is defined by comparing the integrals of the different contributions in the region included between the cut on  $DCA_{xy}$  implemented in the track selection. For the ITS case, it is

$$DCA_{xy}^{cut}(p_T) = 32.7 + \frac{44.8}{p_T^{1.3}}$$
 (3)

In order to extend the primary fraction extraction to higher values of  $p_T$ , where, due to lower statistics, some templates are not populated enough, the distribution is fitted through the function

$$f = \alpha + \beta e^{\gamma x} \tag{4}$$

As an example, Fig. 9 reports a fit for negative pions in the higher multiplicity bin.

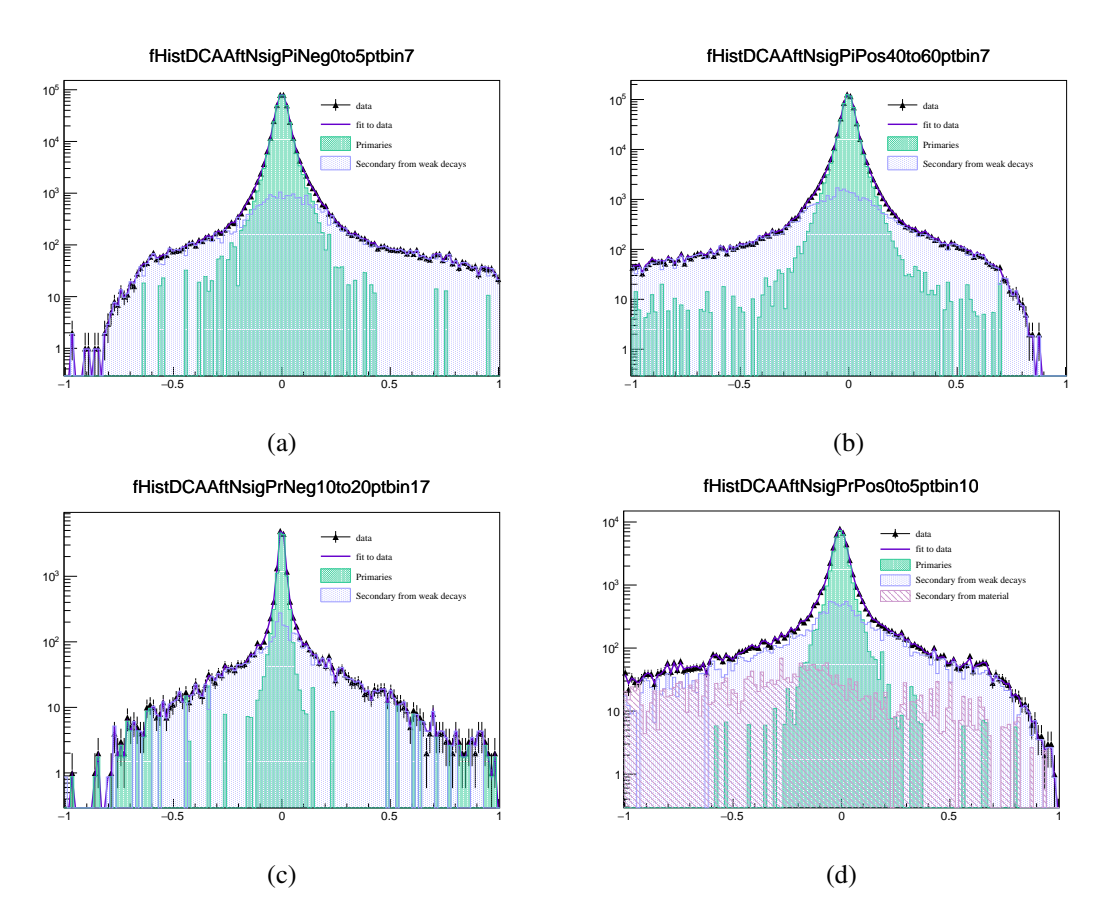


Fig. 6: Fit to the  $DCA_{xy}$  distributions on data for positive (a) and negative (b) pions, negative (c) and positive (d) protons. Different contributions appear: primaries, secondary from weak decay and - for positive protons only - secondary from materials (see legends on plots). Please note that, while the first three histograms refer to a given multiplicity and  $p_T$  bin, plot (d) is integrated in multiplicity.

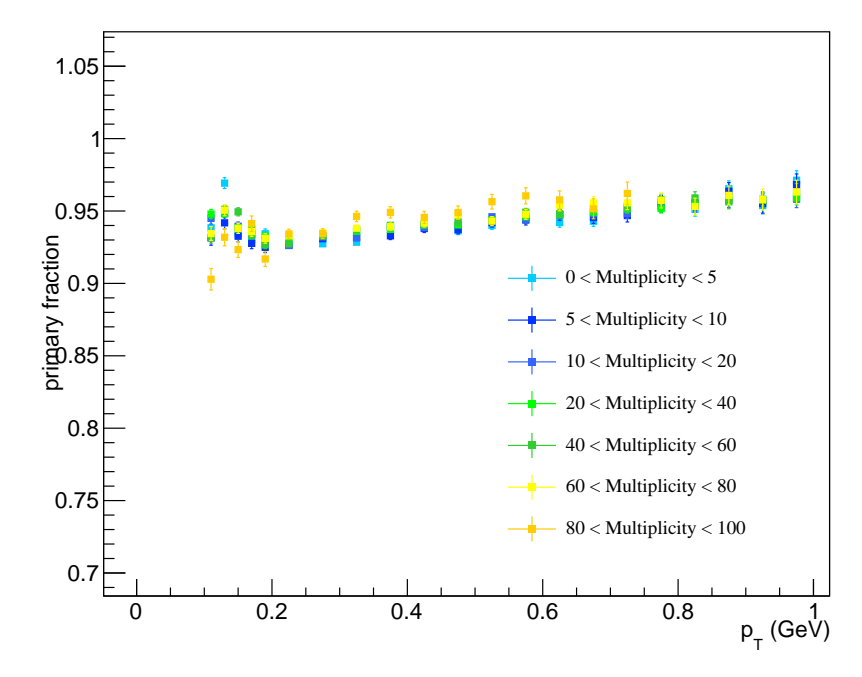


Fig. 7: Dependence on multiplicity of the primary fraction for positive pions.

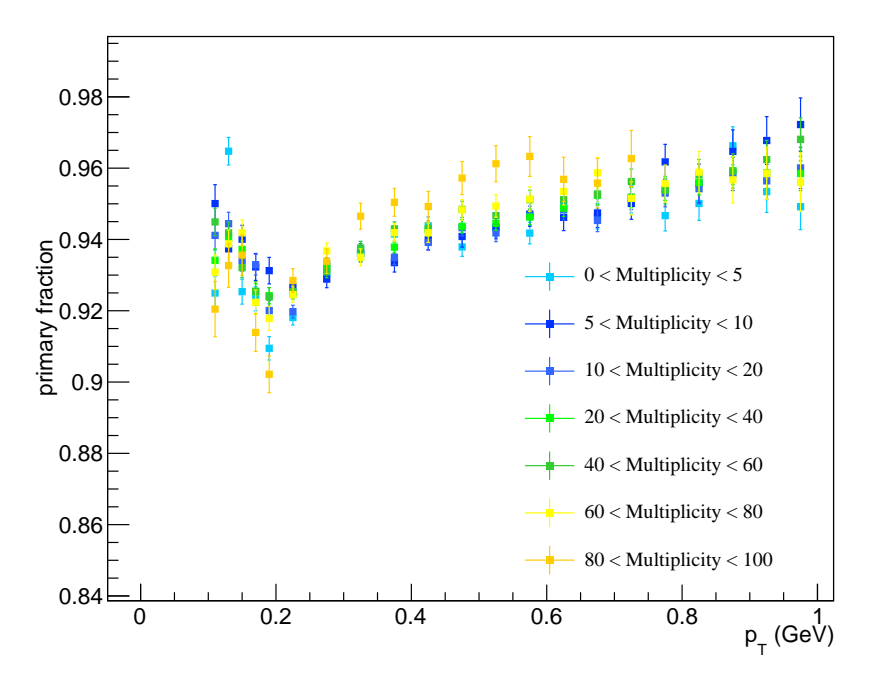


Fig. 8: Dependence on multiplicity of the primary fraction for negative pions.

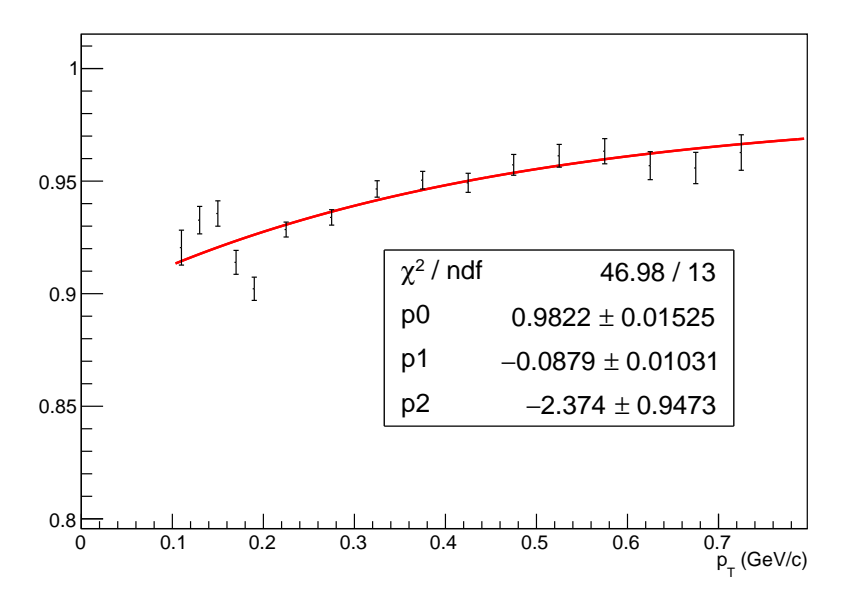


Fig. 9: Example fit to the primary fraction distribution vs.  $p_T$  for negative pions.

# 3.5 Systematic uncertainties

The systematic uncertainties for the spectra extraction are estimated by performing the following checks:

- 1. Varying the track cuts:
  - (a) Number of ITS clusters: **1 (SPD) + 3 (SDD+SSD)**, 2 (SPD) + 4 (SDD+SSD), 1 (SPD) + 4 (SDD+SSD);
  - (b)  $\chi^2/N_{cls}$ : **2.5**, 5;
  - (c) DCA cuts:  $7\sigma$ ,  $5\sigma$ ,  $10\sigma$ ;
- 2. PID method: the Bayesian PID method is used for the estimation of the PID uncertainty (Fig. 10);
- 3.  $V_z$  requirement of the event selection:  $V_z < 10$  cm,  $V_z < 7.5$  cm,  $V_z < 12.5$  cm;
- 4.  $E \times B$ ;
- 5. Pseudo-efficiency check;
- 6. Geant-Fluka correction;
- 7. Material budget for the MC simulation;
- 8. Tracking efficiency.

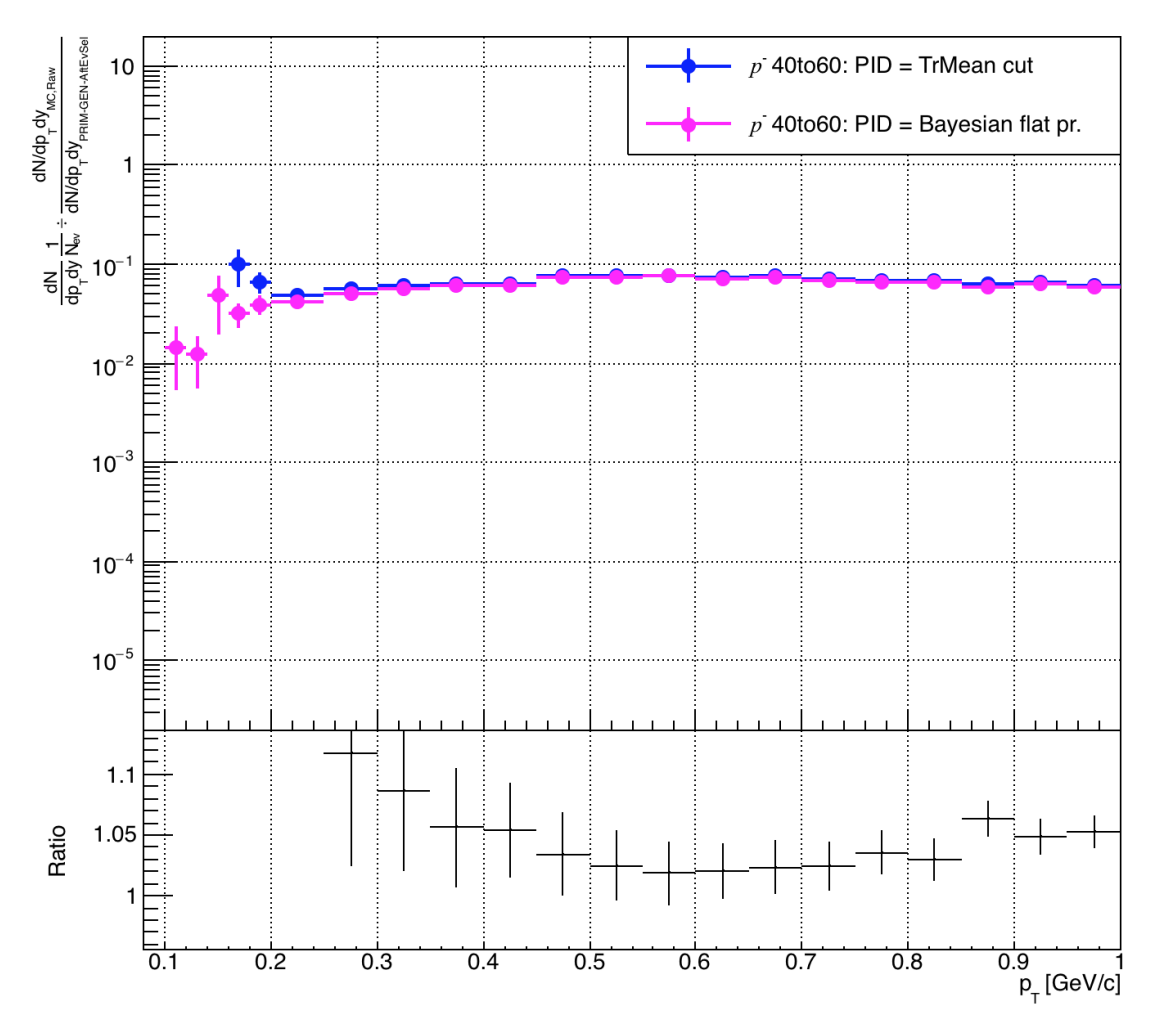


Fig. 10: Preliminary PID systematics for anti-protons in 40to60 multiplicity class, estimated using the Bayesian PID approach with flat priors.

## 4 TPC

The yield extraction with the Time-Projection Chamber is based on the modeling of the energy-loss signal based on the Bethe-Bloch parametrization.

#### 4.1 Track selection

The procedure is applied to tracks that have passed the standard cuts activated through the function

AliESDtrackCuts::GetStandardITSTPCTrackCuts2015PbPb(kTRUE, 1)

that correspond to the following cuts:

- 1. SetMinNCrossedRowsTPC(70)
- 2. SetMinRatioCrossedRowsOverFindableClustersTPC(0.8)
- 3. SetCutGeoNcrNcl(2., 130., 1.5, 0.0, 0.0)
- 4. SetMaxChi2PerClusterTPC(4)
- SetAcceptKinkDaughters(kFALSE)
- SetRequireTPCRefit(kTRUE)
- 7. SetRequireITSRefit(kTRUE)
- 8. SetClusterRequirementITS(AliESDtrackCuts::kSPD, AliESDtrackCuts::kAny)
- 9. SetMaxDCAToVertexXYPtDep("0.0105+0.0350/pt ^ 1.1")
- 10. SetMaxChi2TPCConstrainedGlobal(36)
- 11. SetMaxDCAToVertexZ(2)
- 12. SetDCAToVertex2D(kFALSE)
- 13. SetRequireSigmaToVertex(kFALSE)
- 14. SetMaxChi2PerClusterITS(36)

# **4.2** TPC-based yield extraction in the low- $p_T$ part: fit to $N_{\sigma}$

In the low- $p_T$  part, the energy loss per unit path lenght dE/dx = f(p/m) of charged particles by ionization processes changes rapidly, leading to a good separation among  $\pi^{\pm}$ ,  $\kappa^{\pm}$  and  $p^{\pm}$  in this part of the spectrum. The yield extraction is based on the quantity  $N_{\sigma}$ , defined as

$$N_{\sigma,i} = \frac{dE/dx_{exp,i} - dE/dx_{meas,i}}{dE/dx_{meas,i}}$$
(5)

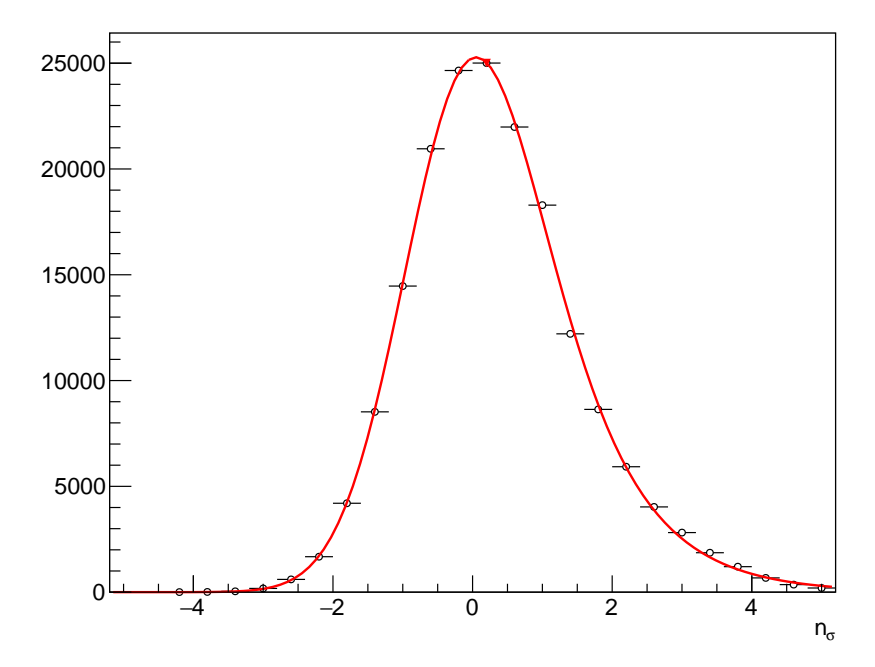


Fig. 11: Fit with a convolution of a Gaussian and a Erfc function to the  $N_{\sigma}$  distribution for  $\pi^{+}$  in 20% < multiplicity < 30% and for  $0.8 < p_{T} < 0.85$  GeV/c. The right tail is described through the contribution of the Erfc component.

that quantifies the distance among the measured energy loss by a particle of specie i to the theoretical value expected from the Bethe-Bloch modeling for a particle of mass  $m_i$ . The raw yields are extracted by fitting the  $N_{\sigma}$  distribution. For any particle species present in the distribution, a Gaussian convoluted with a Erfc function is used as the fitting function. Where the contamination gets higher and a superimposition between two peaks appears, two convoluted functions are used. As an example, in Fig. 11 the fit to the  $N_{\sigma}$  distribution for  $\pi^+$  for 20% < multiplicity < 30% and  $0.8 < p_T < 0.85 \text{ GeV}/c$  are shown, while Fig. 12 shows the same for  $\kappa^+$  in 10% < multiplicity < 20% and for  $0.65 < p_T < 0.7 \text{ GeV}/c$ . In the latter, the contamination from pions is observed. Through this fit, the raw yields are extracted by considering the integral of the signal function (the one centered at zero).

# 4.3 Raw spectra

Through the procedure described in Sec. 4.2 the raw spectra for the different particle species are extracted. They correspond to the quantity

$$\frac{d^2N_i}{d\eta dp_T} \tag{6}$$

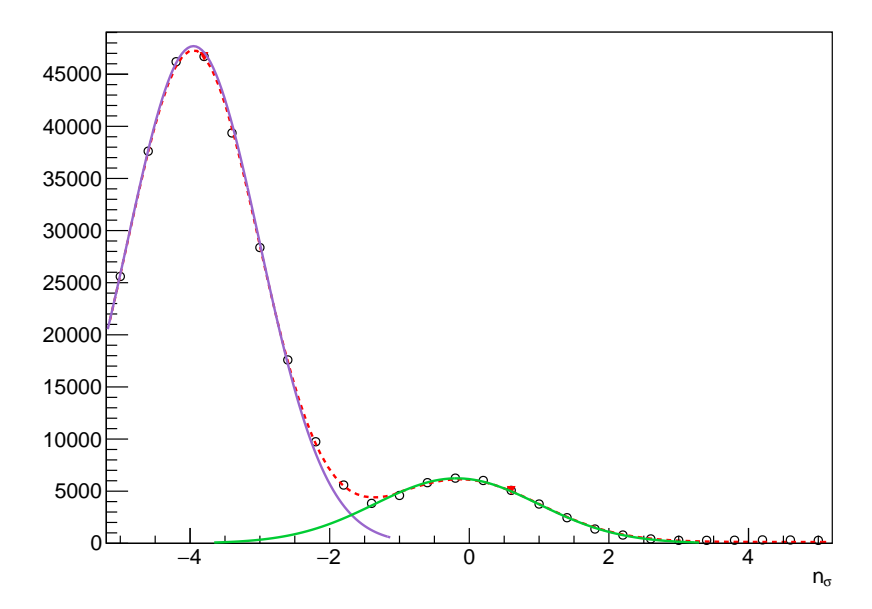


Fig. 12: Fit with two different contribution (pions and kaons) to the  $N_{\sigma}$  distribution for  $\kappa^{+}$  in 10% < multiplicity < 20% and for 0.65 <  $p_{T}$  < 0.7 GeV/c. The right tail is described through the contribution of the Erfc component.

#### 4.4 Particle ratios

Positive to negative particle ratios are shown in Figs. 19, 20 and 21.

### 4.5 Corrections

In order to get the final spectra, raw yields have to be corrected for different effects. Below, the corrections applied are listed and described.

# 4.5.1 Efficiency correction

Efficiencies are calculated through the Monte Carlo production LHC17f3a\_cent\_fix and are defined as the ratio:

$$\varepsilon = \frac{N_{rec.primary}}{N_{gen}} \tag{7}$$

where  $N_{rec.primary}$  is the number of true reconstructed primary tracks and  $N_{gen}$  is the number of generated particles. Tracking efficiencies for *primary particles* are calculated considering the cut

AliESDtrackCuts::GetStandardITSTPCTrackCuts2015PbPb(kTRUE, 1)

Integrated efficiencies for the different species are shown in Fig. 22, respectively for positive (left) and negative (rigth) charged particles. Due to the kaon decay length ( $c\tau \approx 3.7$ m) a drop in efficiency for this species is observed at low  $p_T$ , while the effect is reduced for pions, due to their

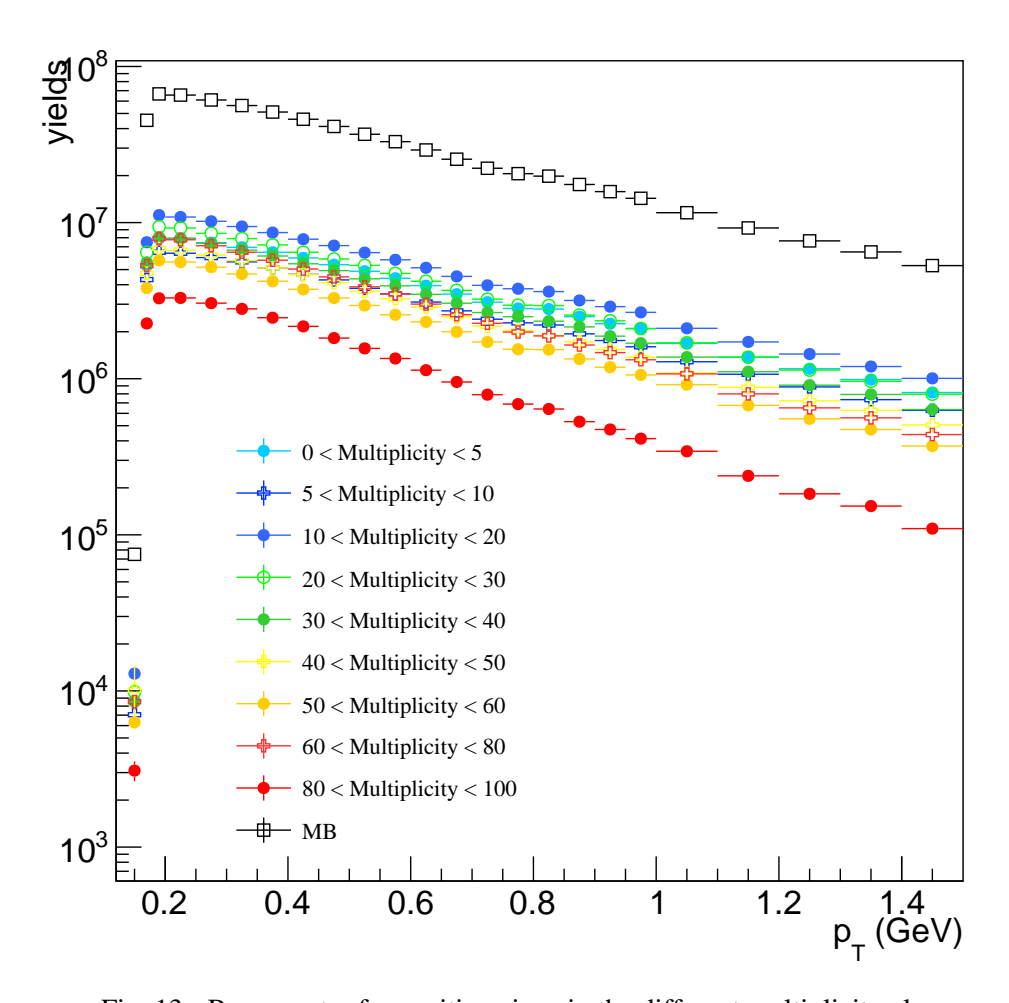


Fig. 13: Raw spectra for positive pions in the different multiplicity classes.

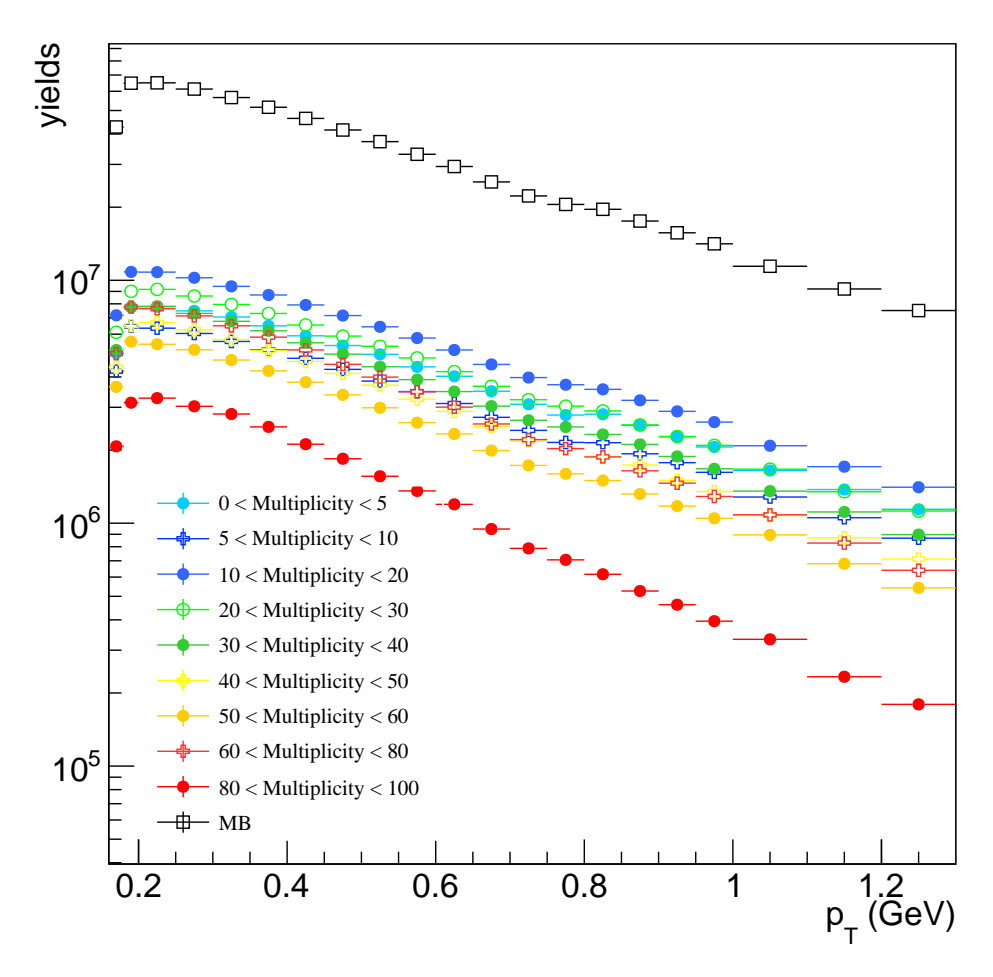


Fig. 14: Raw spectra for negative pions in the different multiplicity classes.

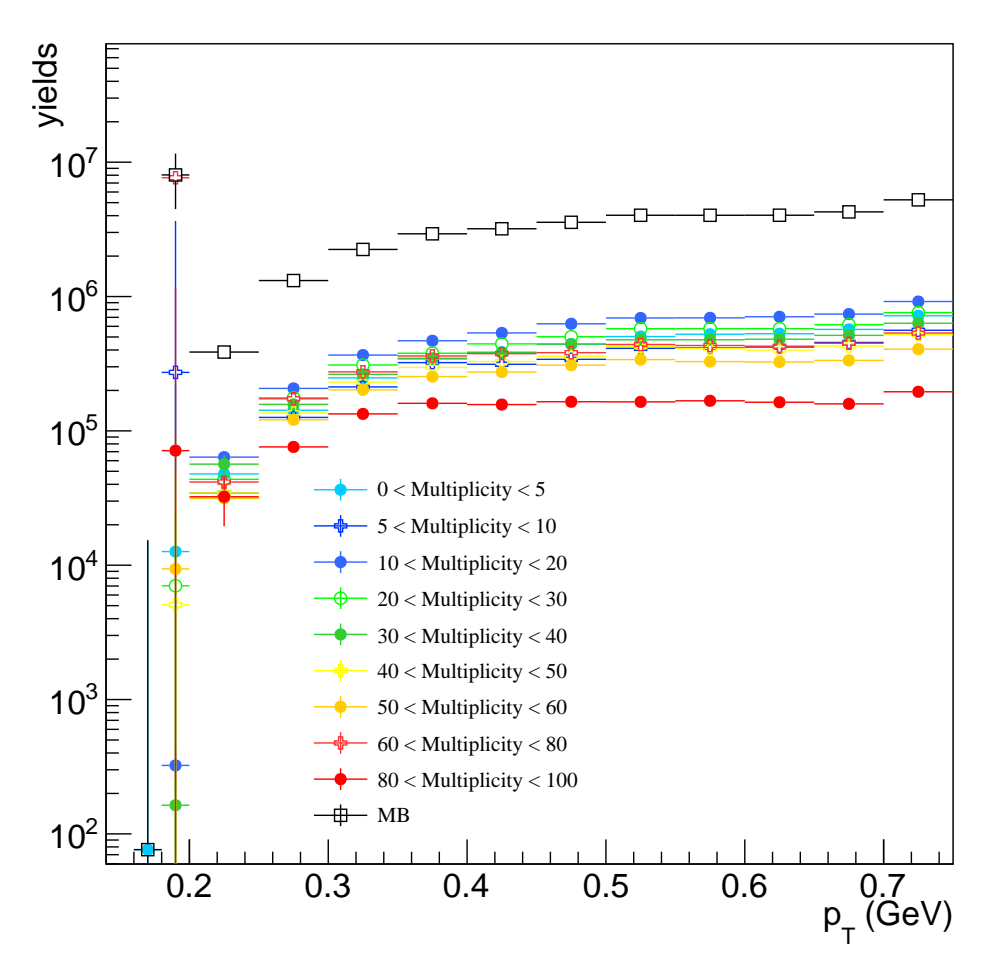


Fig. 15: Raw spectra for positive kaons in the different multiplicity classes.

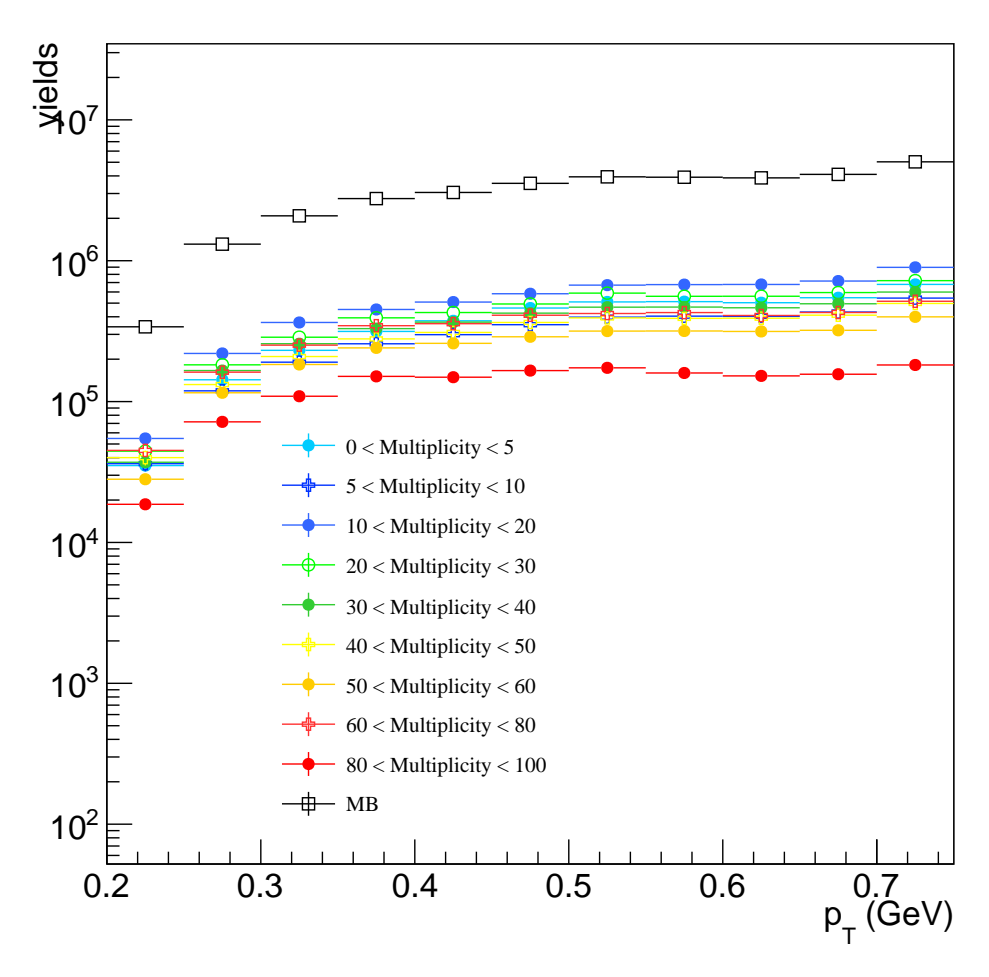


Fig. 16: Raw spectra for negative kaons in the different multiplicity classes.

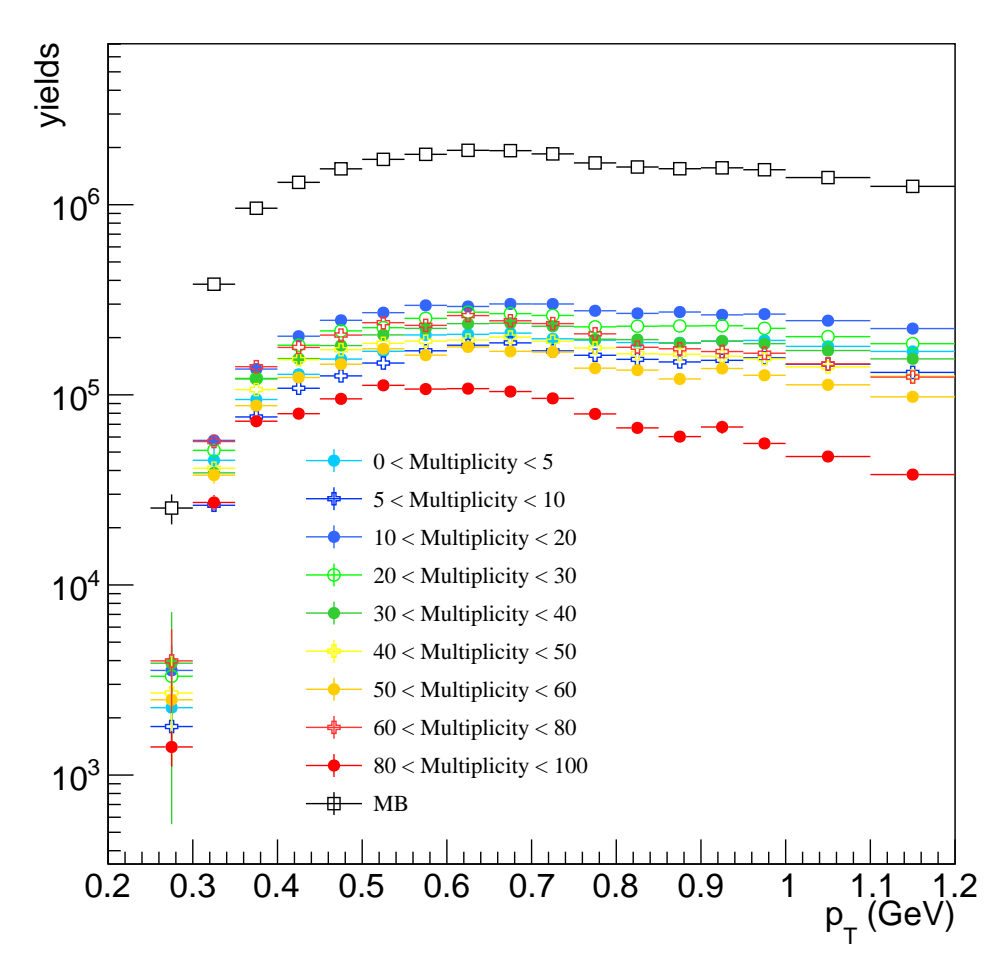


Fig. 17: Raw spectra for positive protons in the different multiplicity classes.

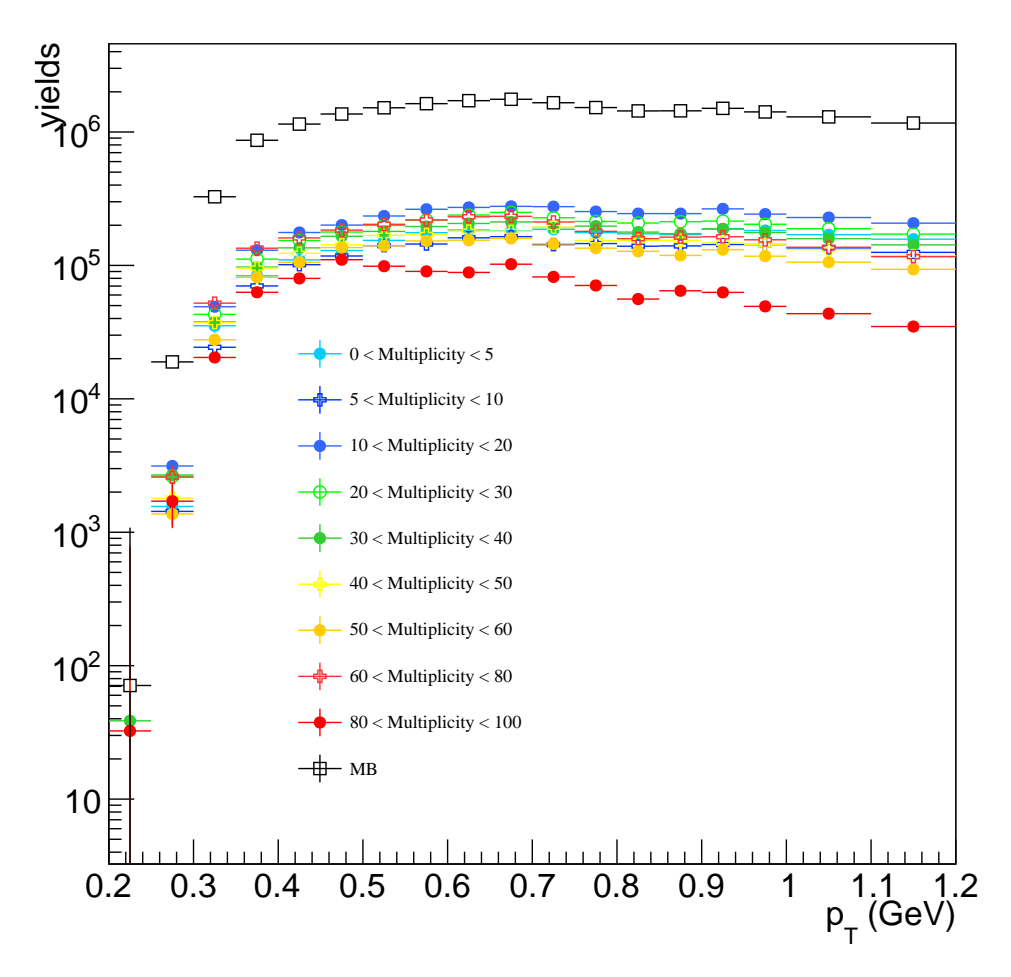


Fig. 18: Raw spectra for antiprotons in the different multiplicity classes.

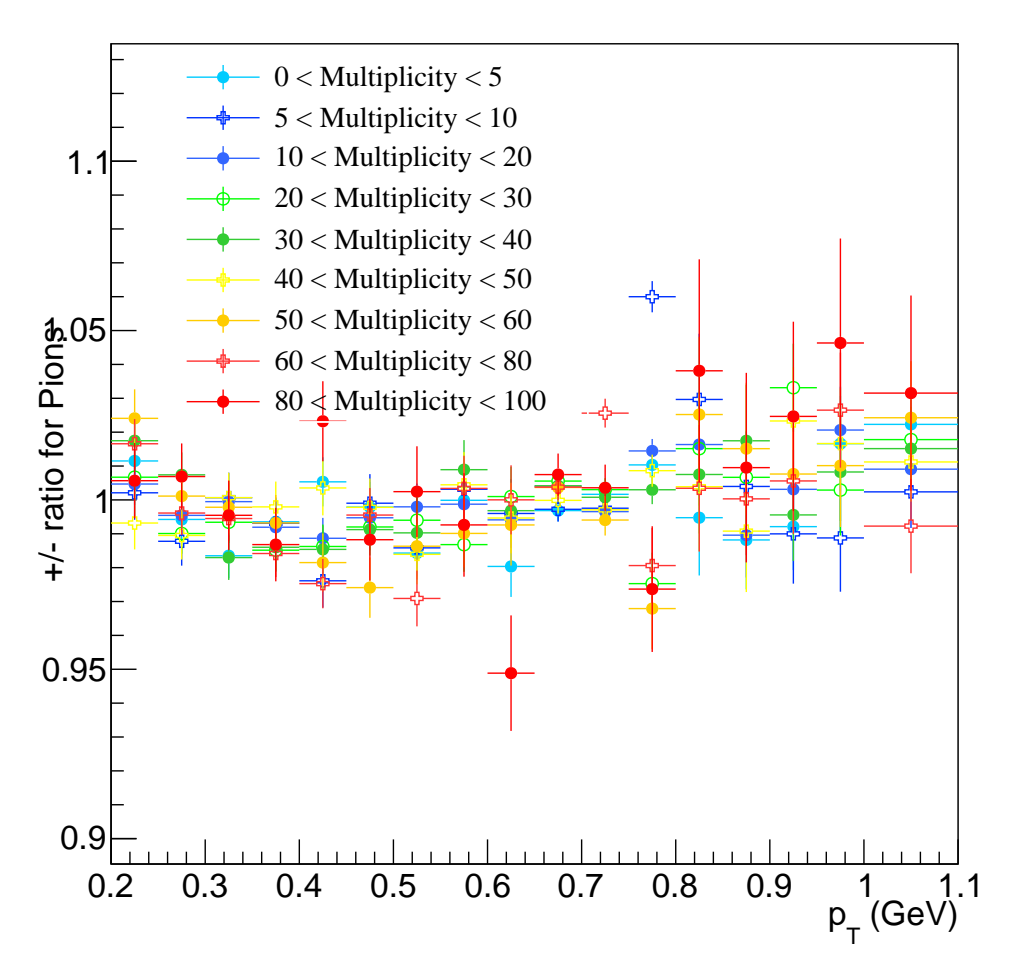


Fig. 19: Positive to negative pion ratios in the different multiplicity classes.

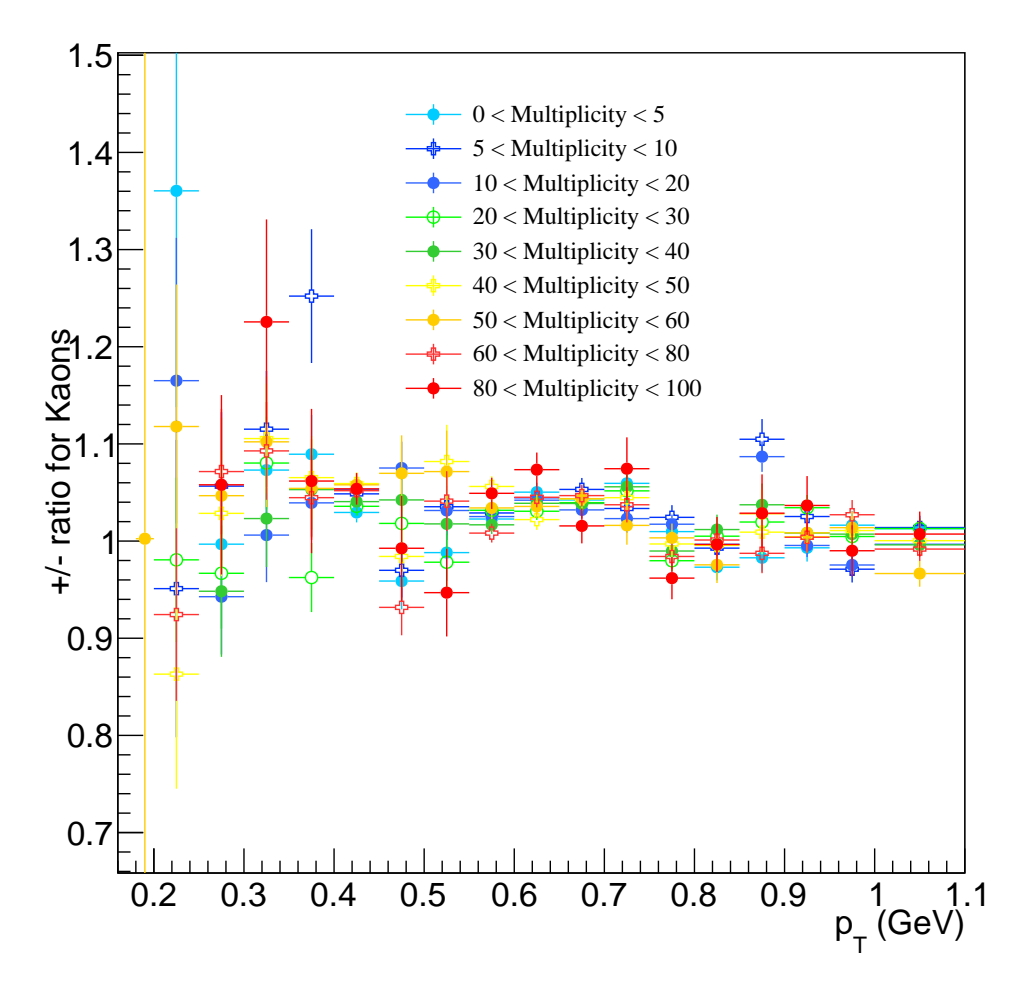


Fig. 20: Positive to negative kaon ratios in the different multiplicity classes.

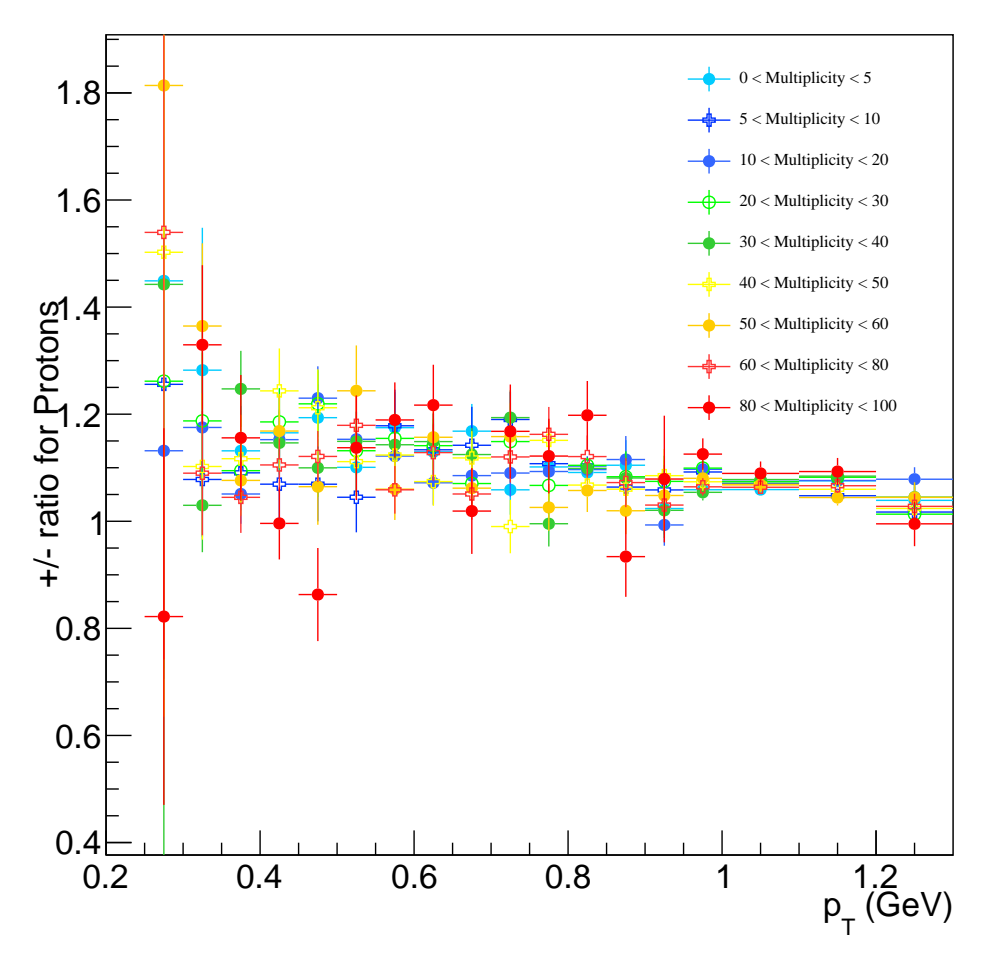


Fig. 21: Positive to negative proton ratios in the different multiplicity classes.

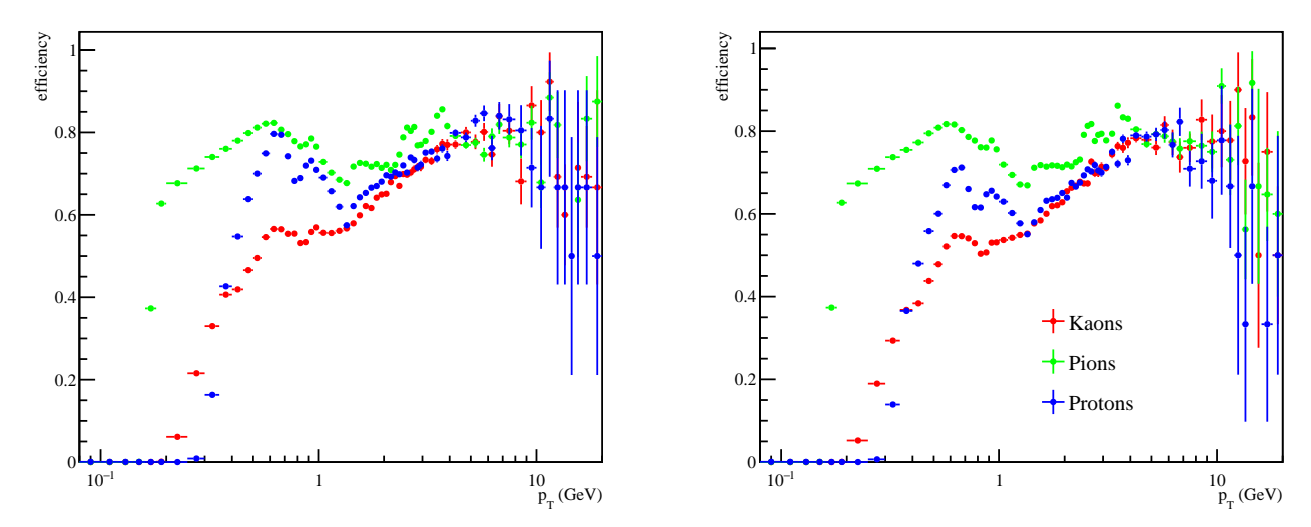


Fig. 22: Efficiencies integrated in multiplicity for the different particle species. Left plot refers to positive particles, right one to negative.

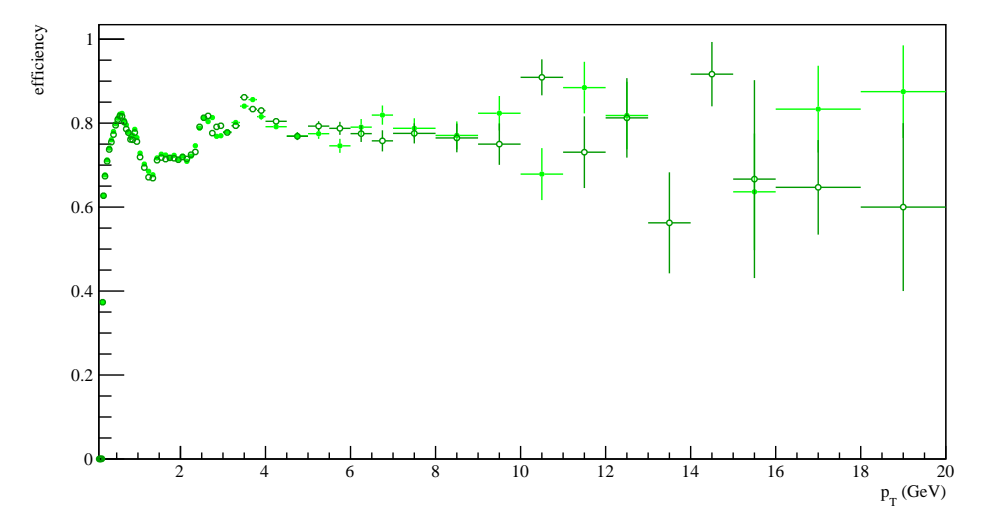


Fig. 23: Efficiencies integrated in multiplicity for for positive (full circle) and negative (empty boxes) pions.

larger lifetime. Efficiencies for different charge states are comparable for pions (see Fig. 23) and kaons (see Fig. 24); for antiprotons (see Fig. 25), a lower efficiency is observed at low- $p_T$  due to hadronic interactions with detector material.

Efficiencies have been also extracted in mutiplicity classes in order to check a possible dependence on the latter. Deviation are of the order of few percent in the region of interest for the TPC analysis, *i.e.* for  $p_T < 1$  GeV. However, efficiency correction are applied in a multiplicity

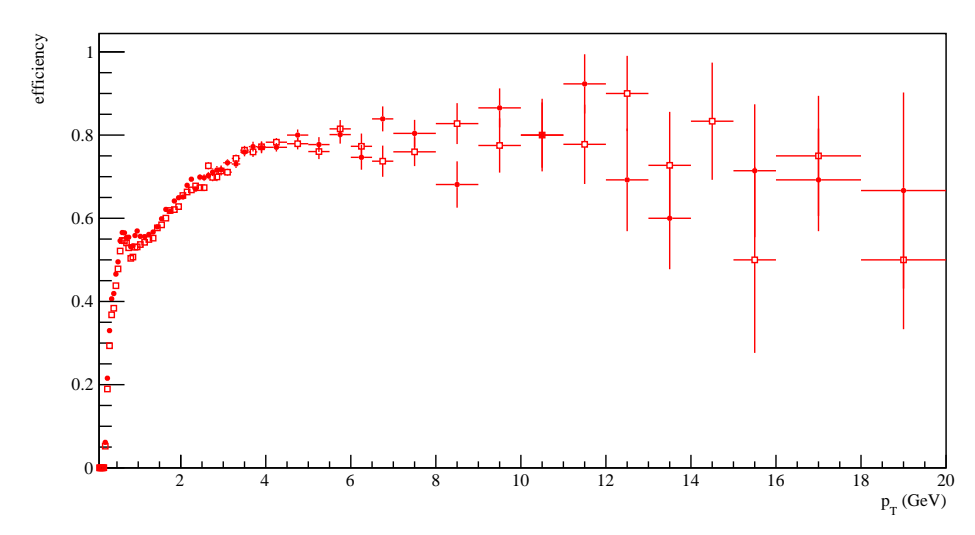


Fig. 24: Efficiencies integrated in multiplicity for for positive (full circle) and negative (empty boxes) kaons.

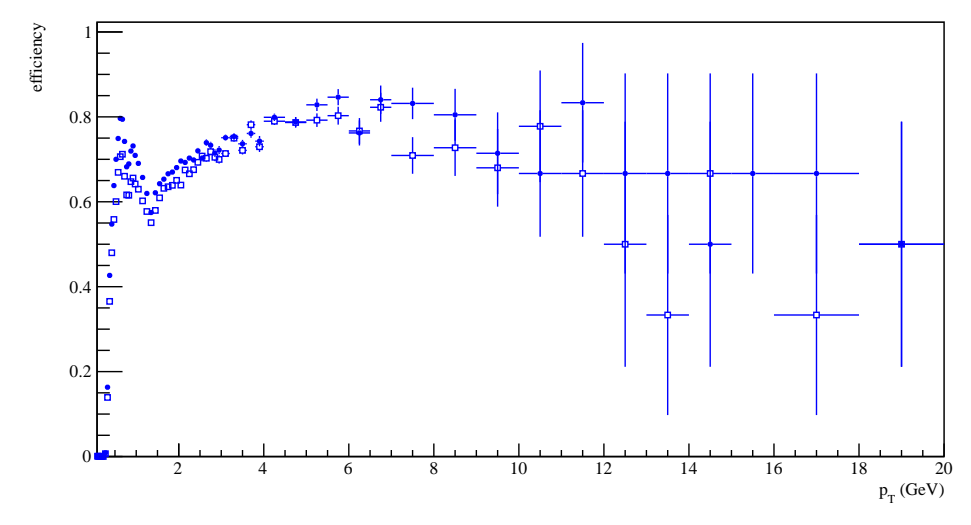


Fig. 25: Efficiencies integrated in multiplicity for for positive (full circle) and negative (empty boxes) protons. The observed lower efficiency for antiprotons in the low- $p_T$  region is due to hadronic interactions.

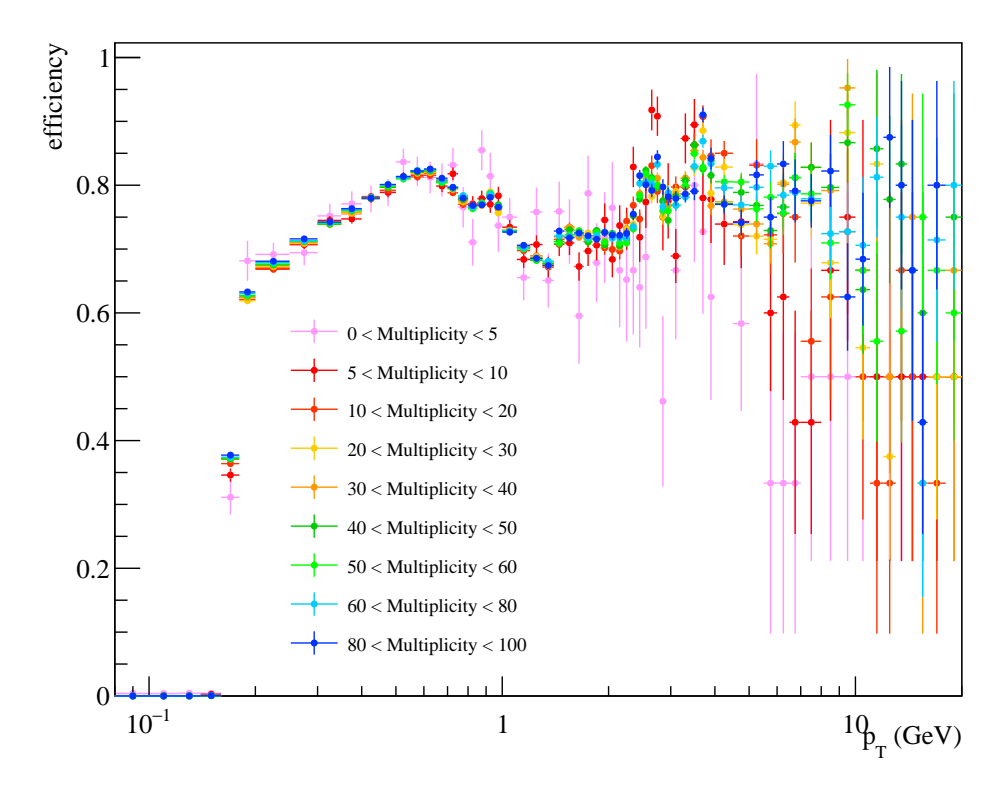


Fig. 26: Efficiencies in multiplicity classes for positive pions.

dependent way.

#### 4.5.2 Geant/Fluka correction

Due to an underestimation of the strangess component in Geant simulation, that led to an underestimation of the secondaries coming from weak decays, a correction is applied to the  $\kappa^-$  spectra to account for such an effect.

#### 4.5.3 Geant3/Geant4 correction

Being the cross-section for antiprotons not properly modeled in the Geant3 implementation, a correction has been introduced by comparing results from Geant3 and Geant4. The correction is applied to antiproton spectra.

## 4.5.4 Primary fraction corrections

Pions and protons in the two charged states are further corrected in order to select only those particles coming from the collisions or produced through strong processes. Secondary particles leading to contamination of secondaries to the final primary sample are produced, e.g., from the weak decay of strange baryons (e.g. in the process  $\Lambda \to \pi p$ ). For protons, a further contribution

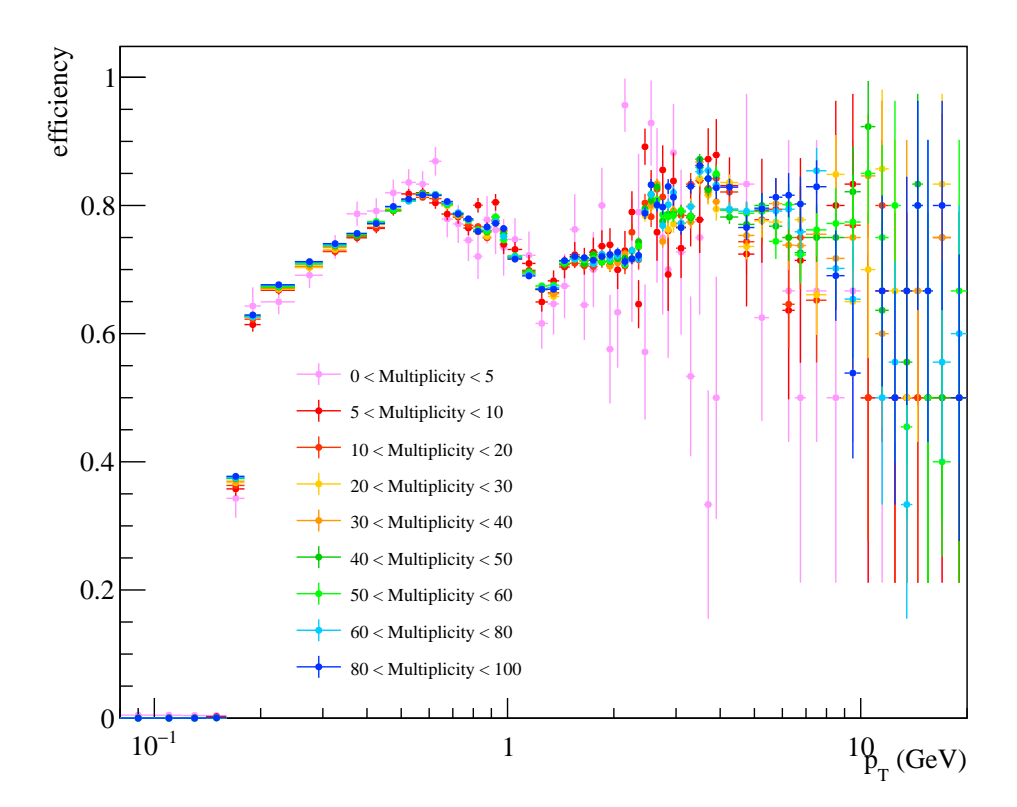


Fig. 27: Efficiencies in multiplicity classes for negative pions.

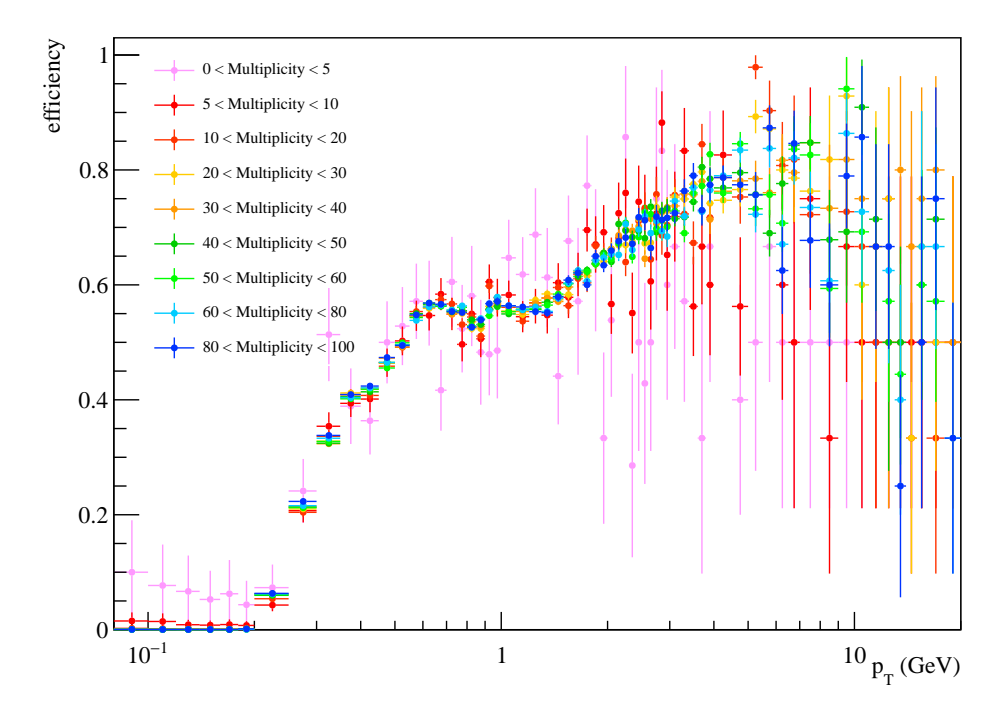


Fig. 28: Efficiencies in multiplicity classes for positive kaons.

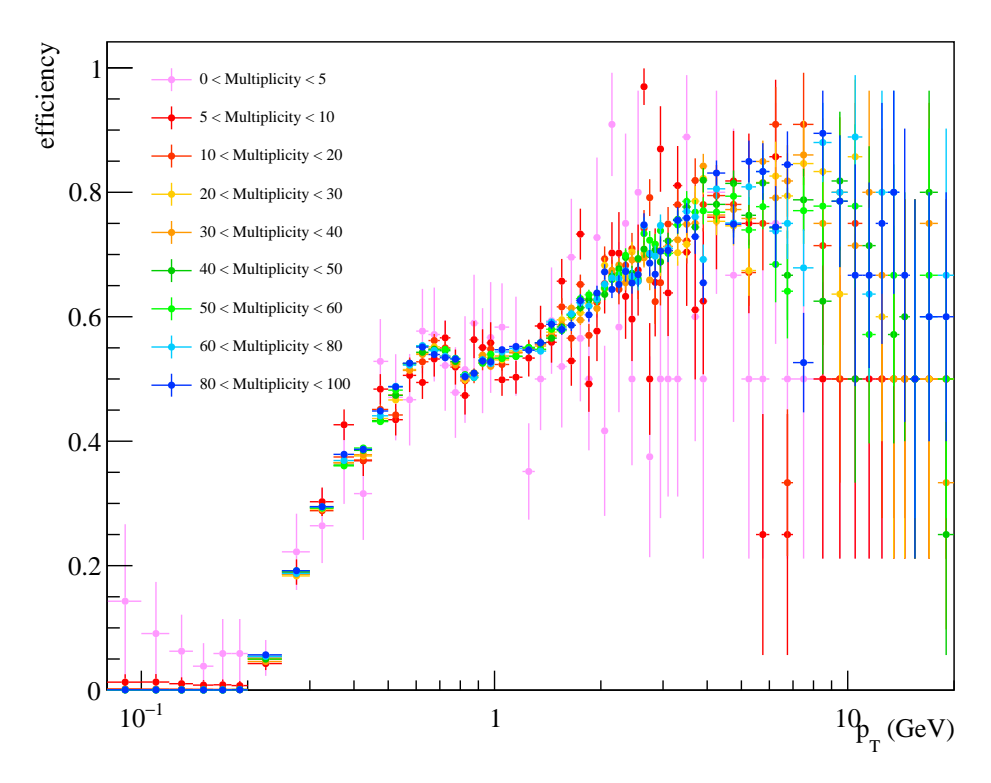


Fig. 29: Efficiencies in multiplicity classes for negative kaons.

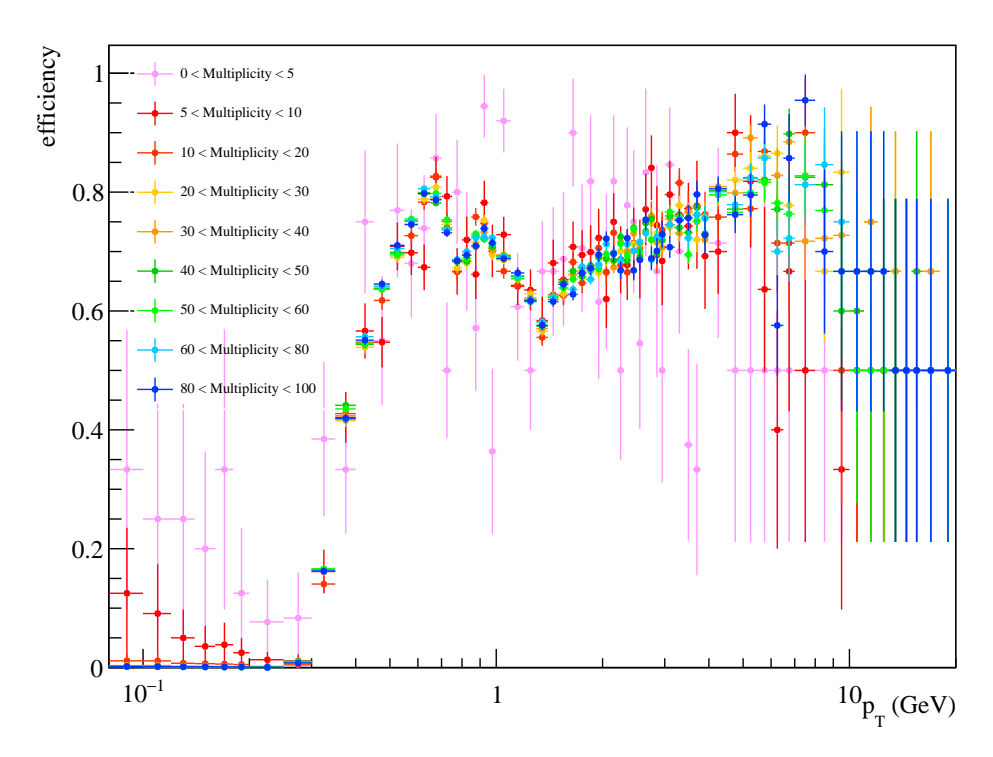


Fig. 30: Efficiencies in multiplicity classes for positive protons.

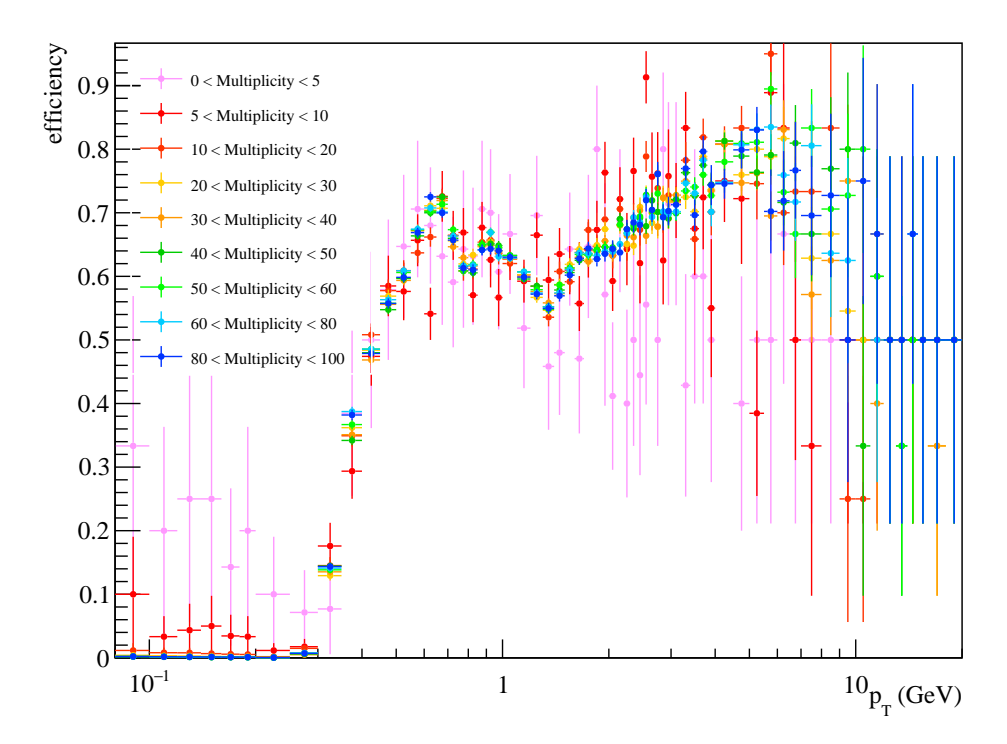


Fig. 31: Efficiencies in multiplicity classes for antiprotons.

has to be considered, namely the protons coming from material that contribute to the final proton sample. In order to extract the different contributions, the distribution of the distance of closest approach in the xy plane ( $DCA_{xy}$ ) is considered. The latter, for data, is produced by adopting the same track cuts described above but for the  $p_T$ -dependent cut on the  $DCA_{xy}$ , that for the present analysis is

$$DCA_{xy}^{cut}(p_T) = 0.0105 + \frac{0.0350}{p_T^{1.1}}$$
(8)

In order to properly produce a template distribution for a given particle specie on data, a  $2-\sigma$  cut on data is applied. As to MC, templates for the different contributions (primaries, secondaries from weak decays, secondary for materials, the latter only for protons) are produced by using information from the Monte Carlo truth. They are then scaled to data in order to describe data distribution as a linear combination of the various components. Performances of the procedure can be appreciated by looking at the distributions of  $DCA_{xy}$  for charged pions (see Figs. 32, 33), anti-protons (see Fig. 34) and protons (see Fig. 35) are shown. The primary fraction for any  $p_T$  and multiplicity bin is then extracted. Multiplicity dependence of the primary fraction distribution vs.  $p_T$  is reported in Fig. 36 ( $\pi^+$ ), Fig. 37 ( $\pi^-$ ), Fig. 38 ( $\bar{p}$ ). For pions, only a slight dependence is observed with multiplicity classes, within a few percent.

In order to extend the primary fraction extraction to higher values of  $p_T$ , where, due to lower statistics, some templates are not populated enough, the distribution is fitted through the function

$$f = \alpha + \beta e^{\gamma x} \tag{9}$$

As an example, Fig. 39 reports a fit for negative pions in the higher multiplicity bin.

#### 4.6 Systematics

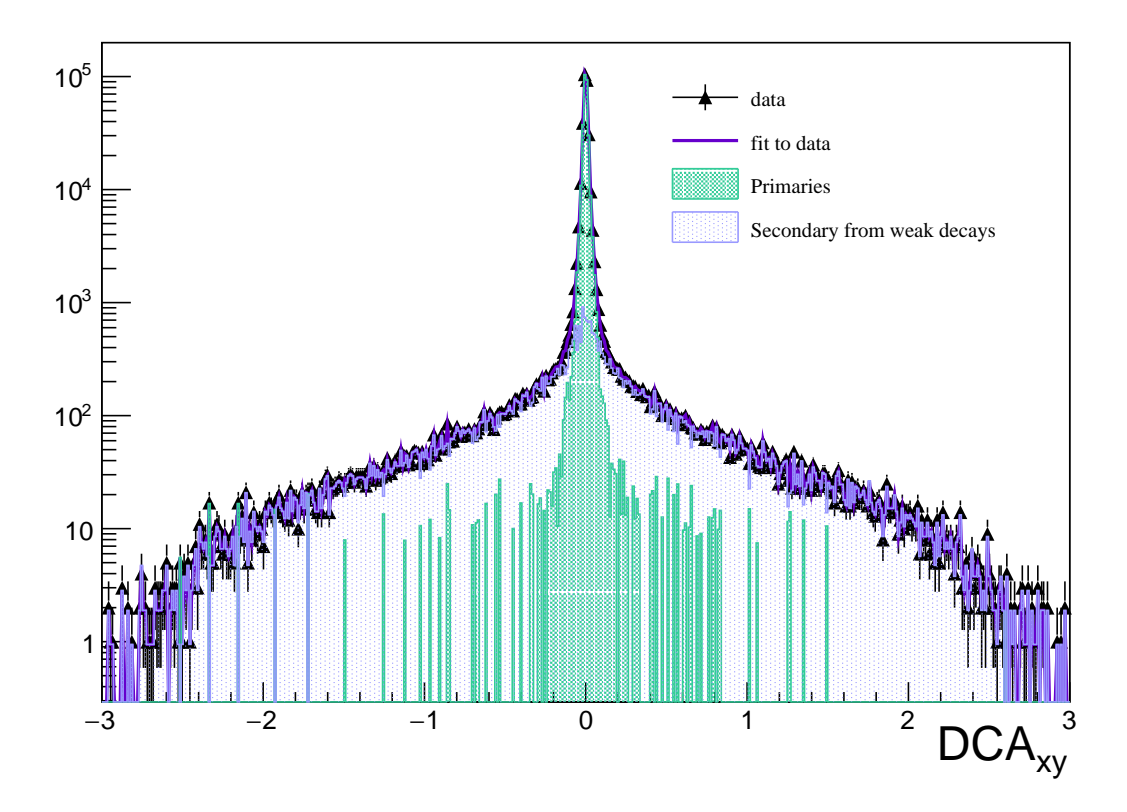
In order to properly account for the different systematics affecting the present analysis, different effects are considered, some related to the event and track selection and others due to the strategy adopted for the yield extraction.

#### 4.6.1 Systematics on event and track selection cuts

To be completed.

#### 4.6.2 Yield extraction

- 1. The strategy adopted in the yield extraction has been varied. Namely, instead of a fit to the  $N_{\sigma}$  distribution, as described in Sec. 4.2, a simple bin counting in the interval  $\pm$  3  $\sigma$  is adopted. Figs. 40 and 41 shows the overall effect for positive and negative pions, respectively. The systematics turns out to be of a few percent, with the alternative approach being almost systematically higher due to the simple bin counting instead of the actual unfolding through the fit, that overestimate the yields. The former approach, in fact, do not take into account possible contaminations from other species, that the fit accounts for.
- 2. the cut on  $DCA_{xy}$  used to extract the feed-down corrections is varied from  $\pm$  3 cm to  $\pm$  1 cm. The difference is adopted as systematics.



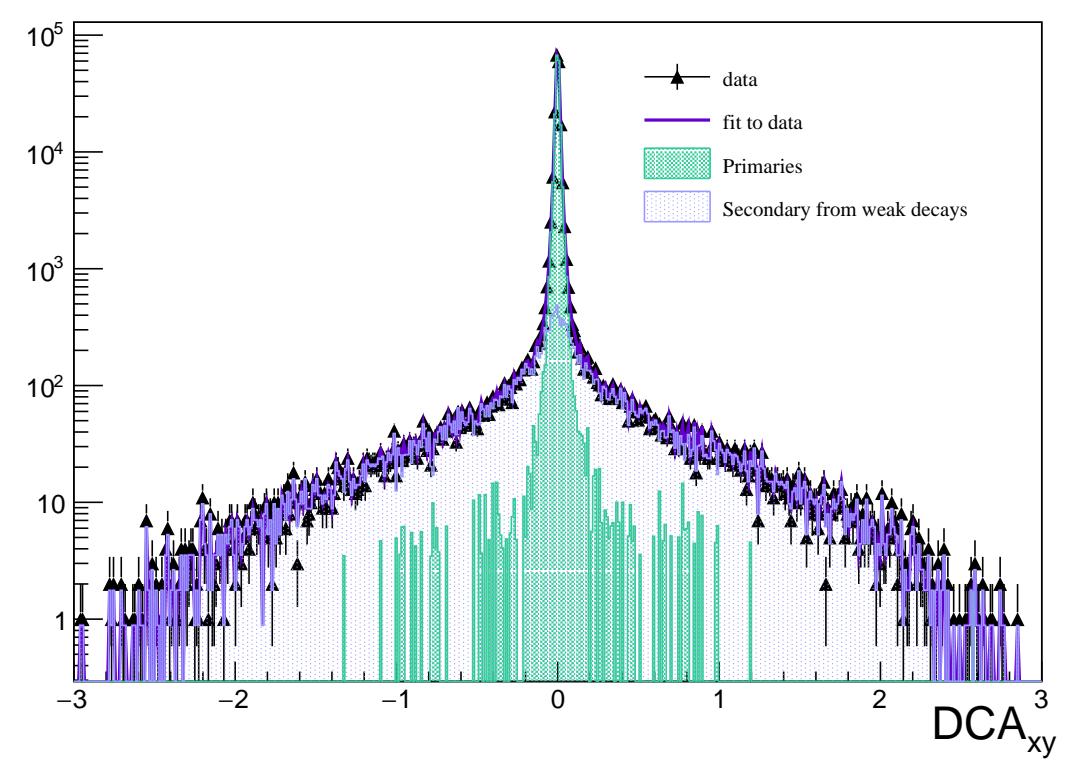
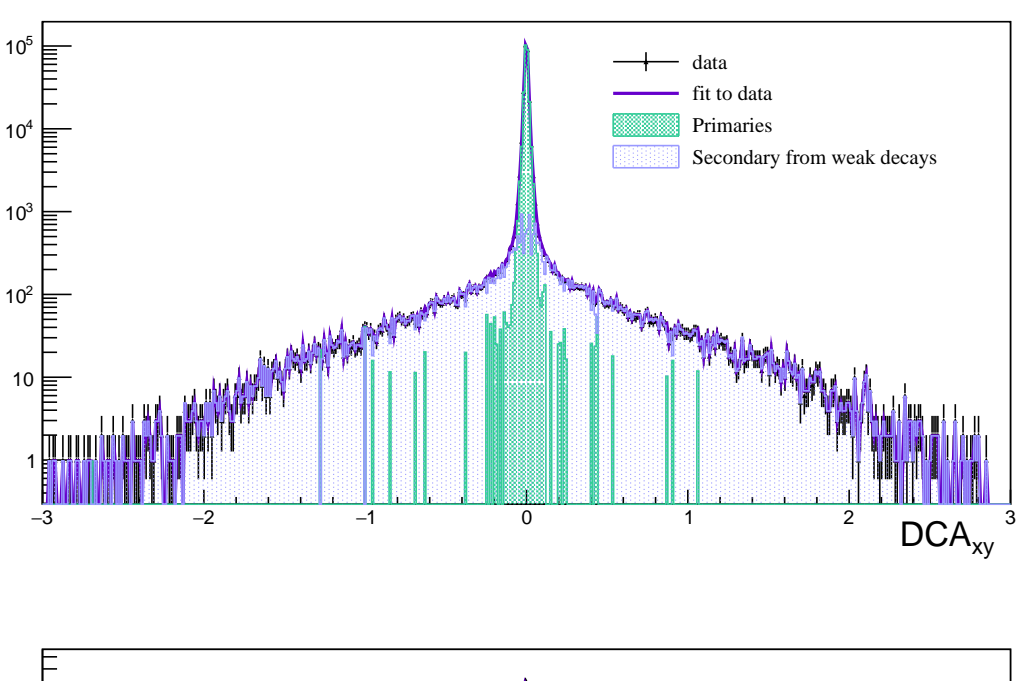


Fig. 32:  $DCA_{xy}$  distribution (in cm) for the different contributions for  $\pi^+$  in the third multiplicity bin and in the  $13^{th}$  p<sub>T</sub> bin (top plot) and in the fourth multiplicity bin and in the  $15^{th}$  p<sub>T</sub> bin (bottom plot). Black triangles represent the distribution on data, produced as described in the text through a 2- $\sigma$  cut; green-filled histogram represents the primary distribution while the violet-shadowed histogram represents the secondary coming from weak decays. Magenta line represents the fit to data.



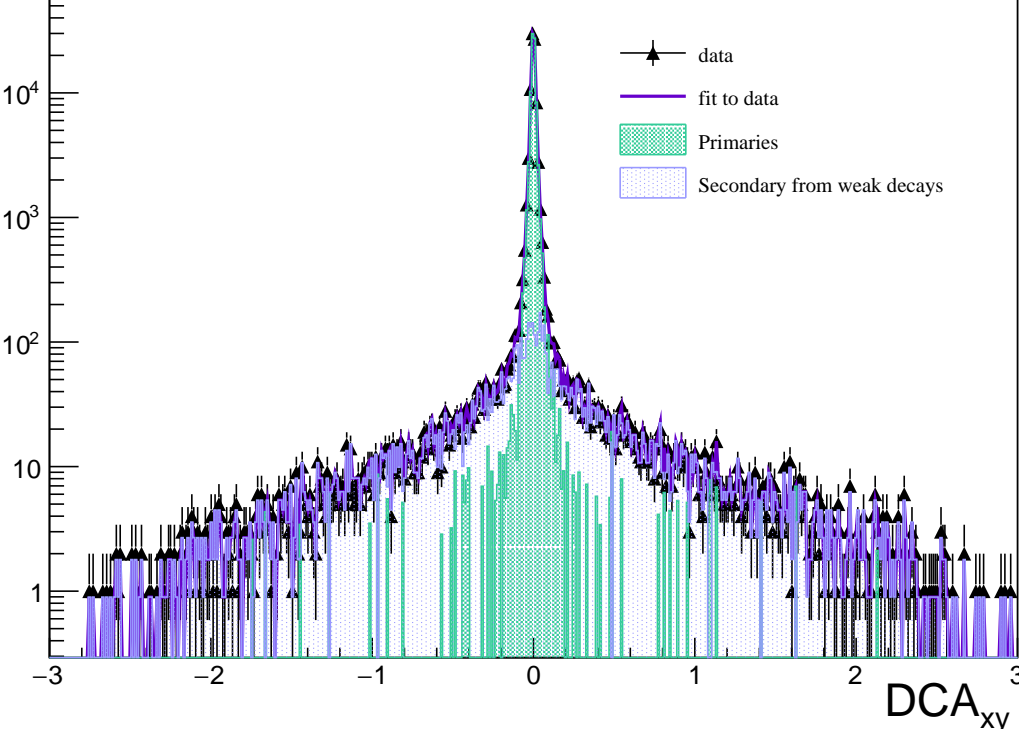
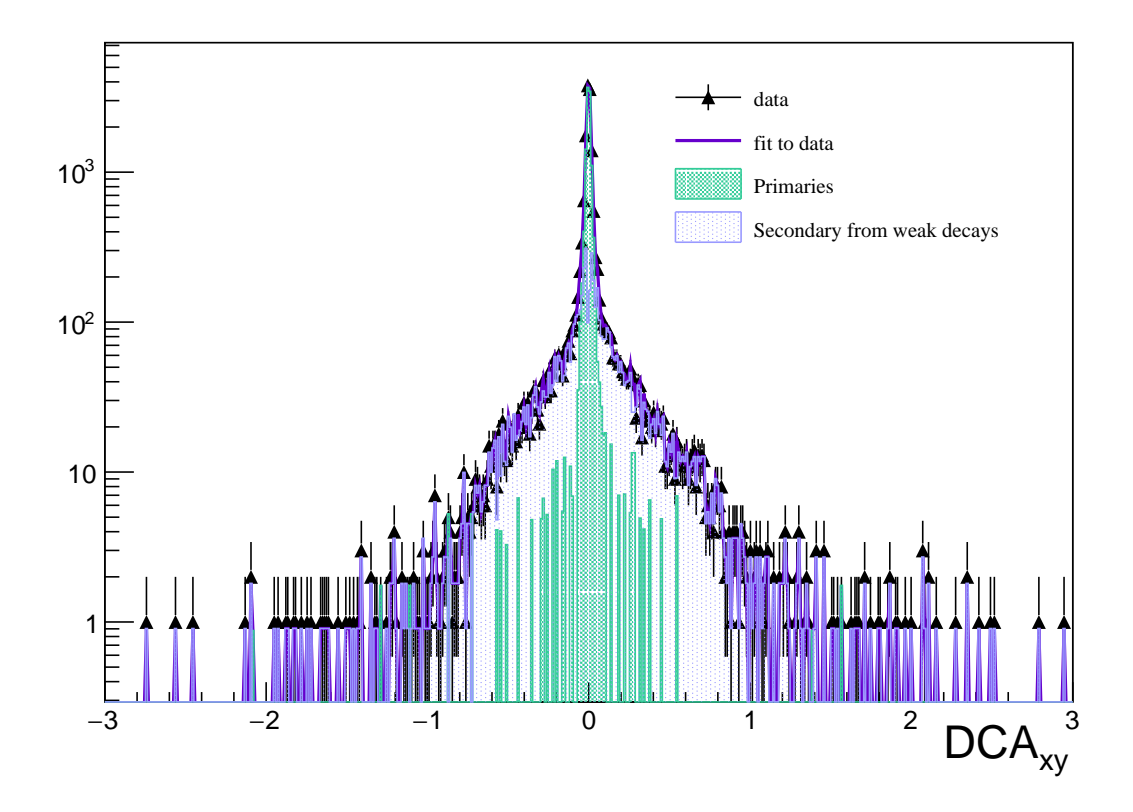


Fig. 33:  $DCA_{xy}$  distribution (in cm) for the different contributions for  $\pi + -$  in the second multiplicity bin and in the  $16^{th}$  p<sub>T</sub> bin (top plot) and in the eight multiplicity bin and in the  $13^{rd}$  p<sub>T</sub> bin (bottom plot). Black triangles represent the distribution on data, produced as described in the text through a 2- $\sigma$  cut; green-filled histogram represents the primary distribution while the violet-shadowed histogram represents the secondary coming from weak decays. Magenta line represents the fit to data.



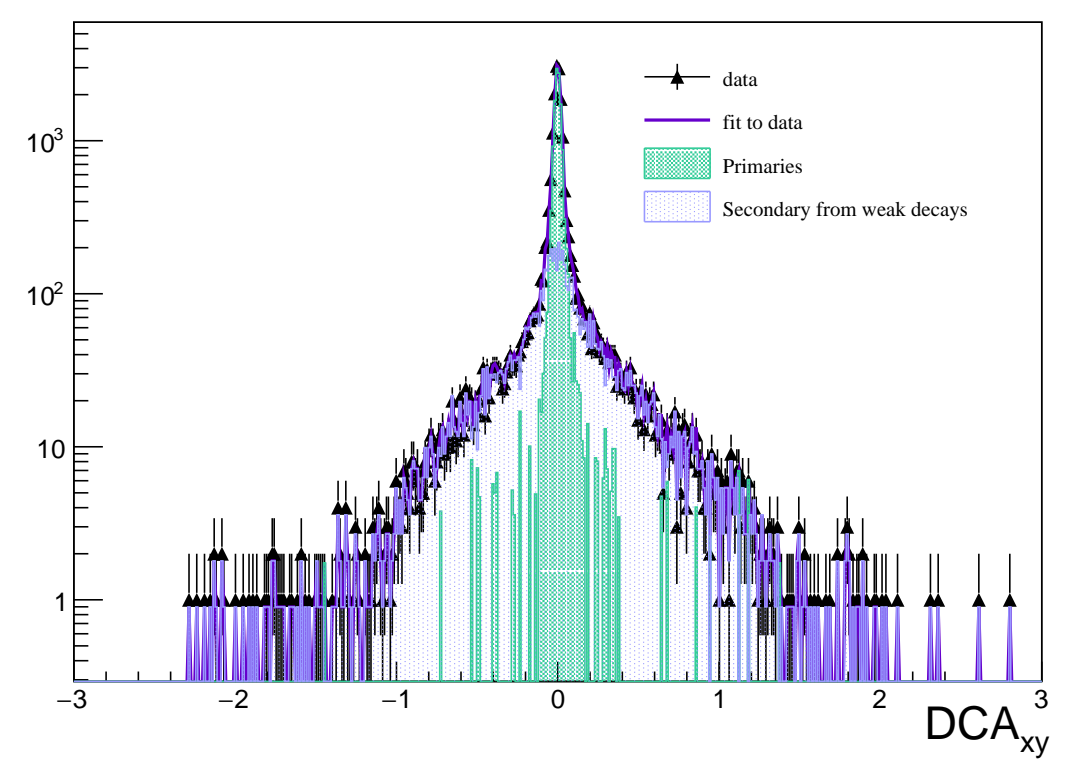


Fig. 34:  $DCA_{xy}$  distribution (in cm) for the different contributions for  $\bar{p}$  in the fourth multiplicity bin and in the  $17^{th}$  p<sub>T</sub> bin (top plot) and in the seventh multiplicity bin and in the  $13^{rd}$  p<sub>T</sub> bin (bottom plot). Black triangles represent the distribution on data, produced as described in the text through a 2- $\sigma$  cut; green-filled histogram represents the primary distribution while the violet-shadowed histogram represents the secondary coming from weak decays. Magenta line represents the fit to data.

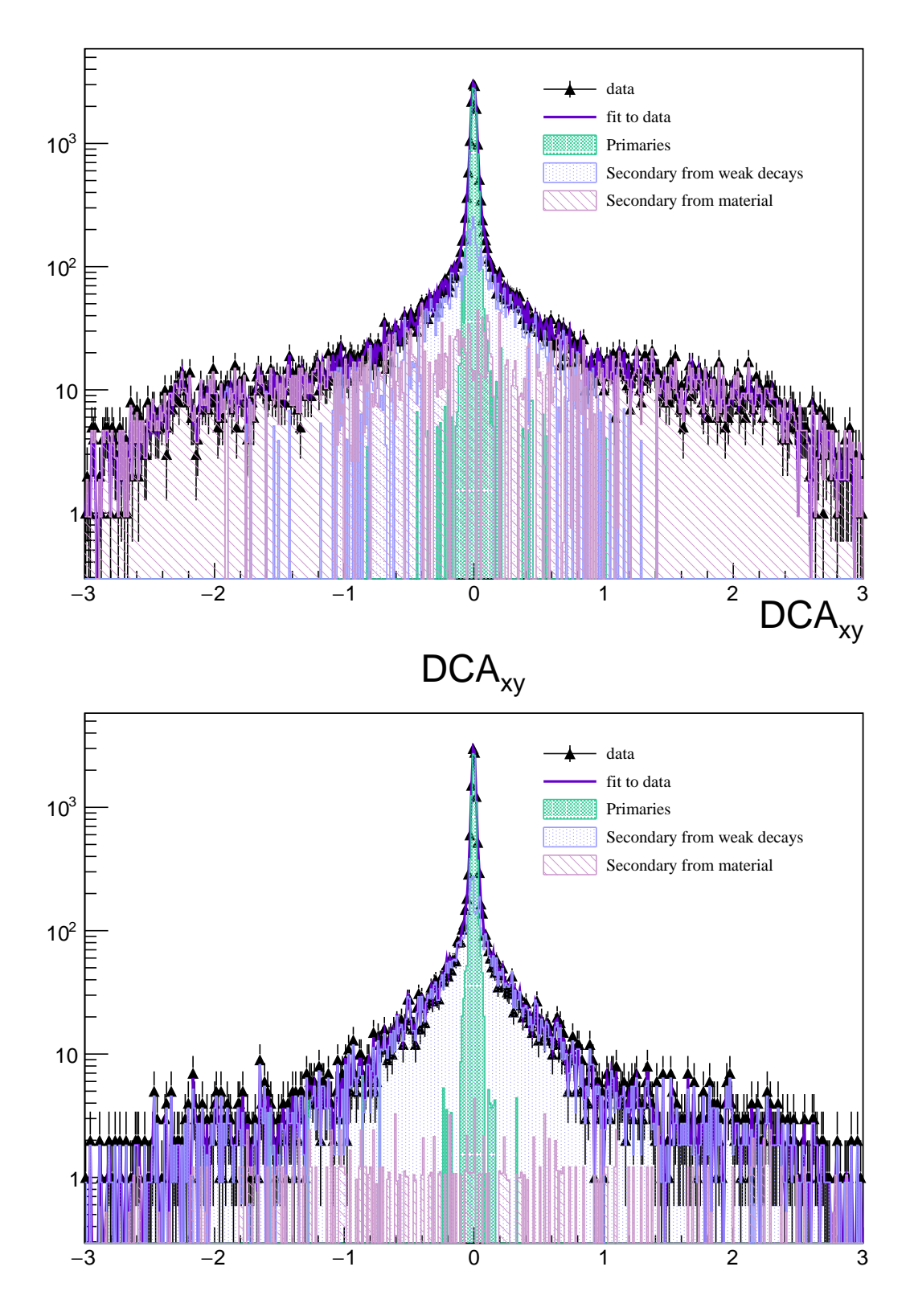


Fig. 35:  $DCA_{xy}$  distribution (in cm) for the different contributions for p in the fourth multiplicity bin and in the  $17^{th}$  p<sub>T</sub> bin (top plot) and in the seventh multiplicity bin and in the  $13^{rd}$  p<sub>T</sub> bin (bottom plot). Black triangles represent the distribution on data, produced as described in the text through a  $2-\sigma$  cut; green-filled histogram represents the primary distribution while the violet-shadowed histogram represents the secondary coming from weak decays. In the proton case, the additional contribution of secondaries from material is considered and shown as pink-filled histogram. Magenta line represents the fit to data.

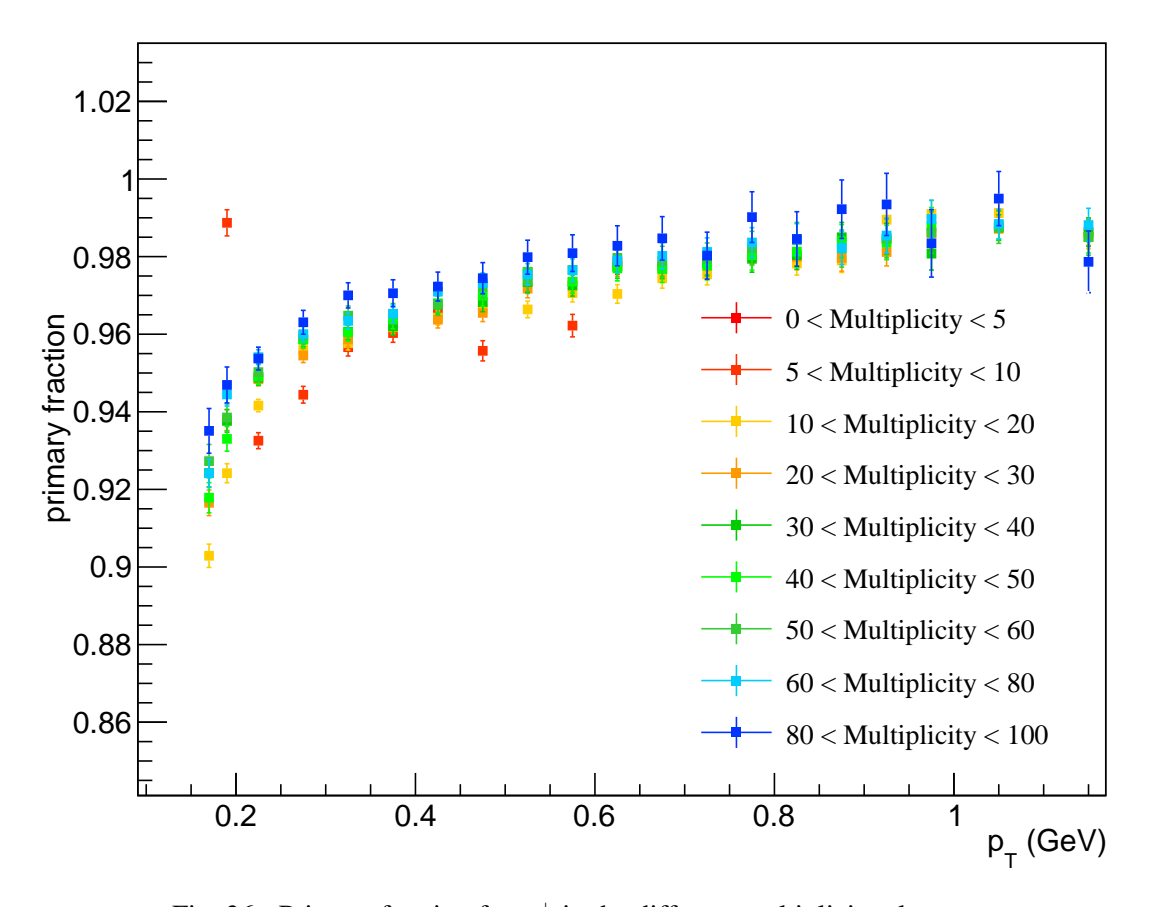


Fig. 36: Primary fraction for  $\pi^+$  in the different multiplicity classes.

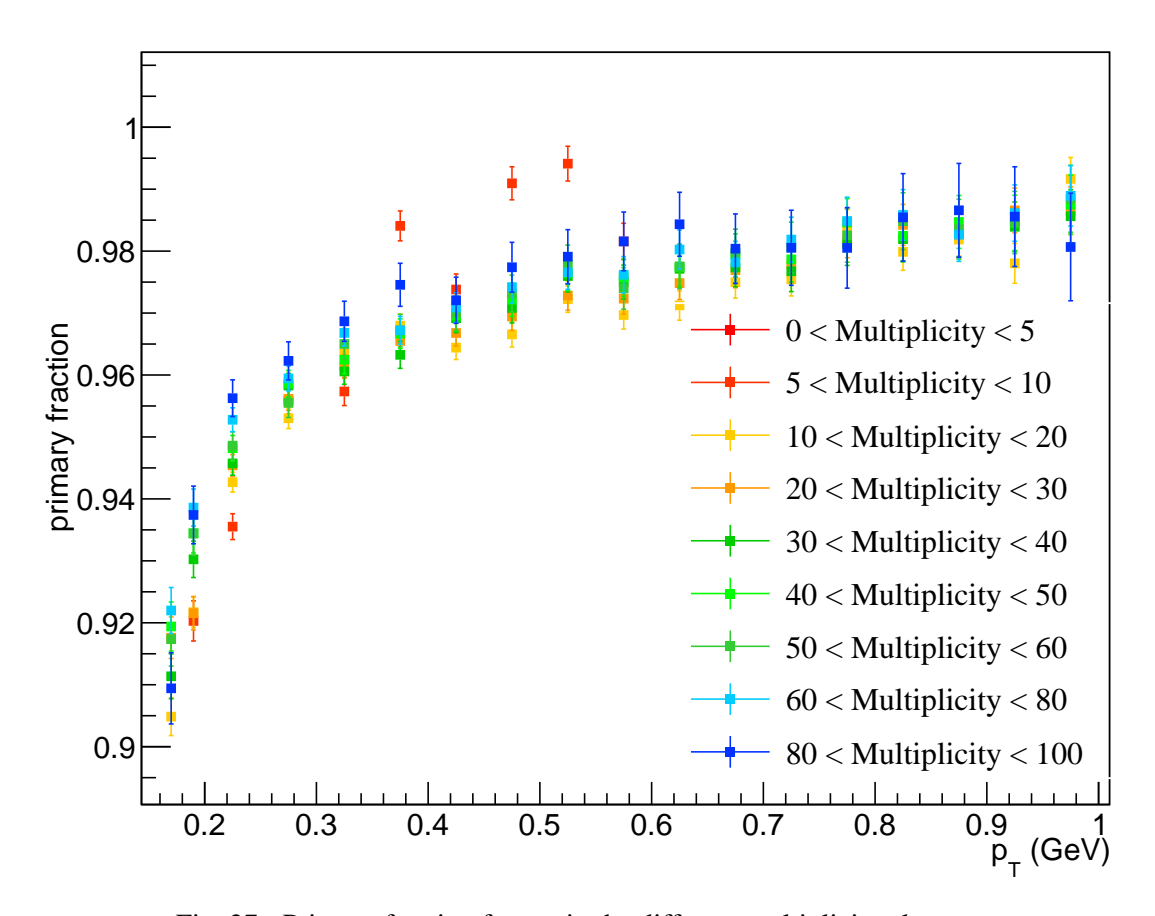


Fig. 37: Primary fraction for  $\pi^-$  in the different multiplicity classes.

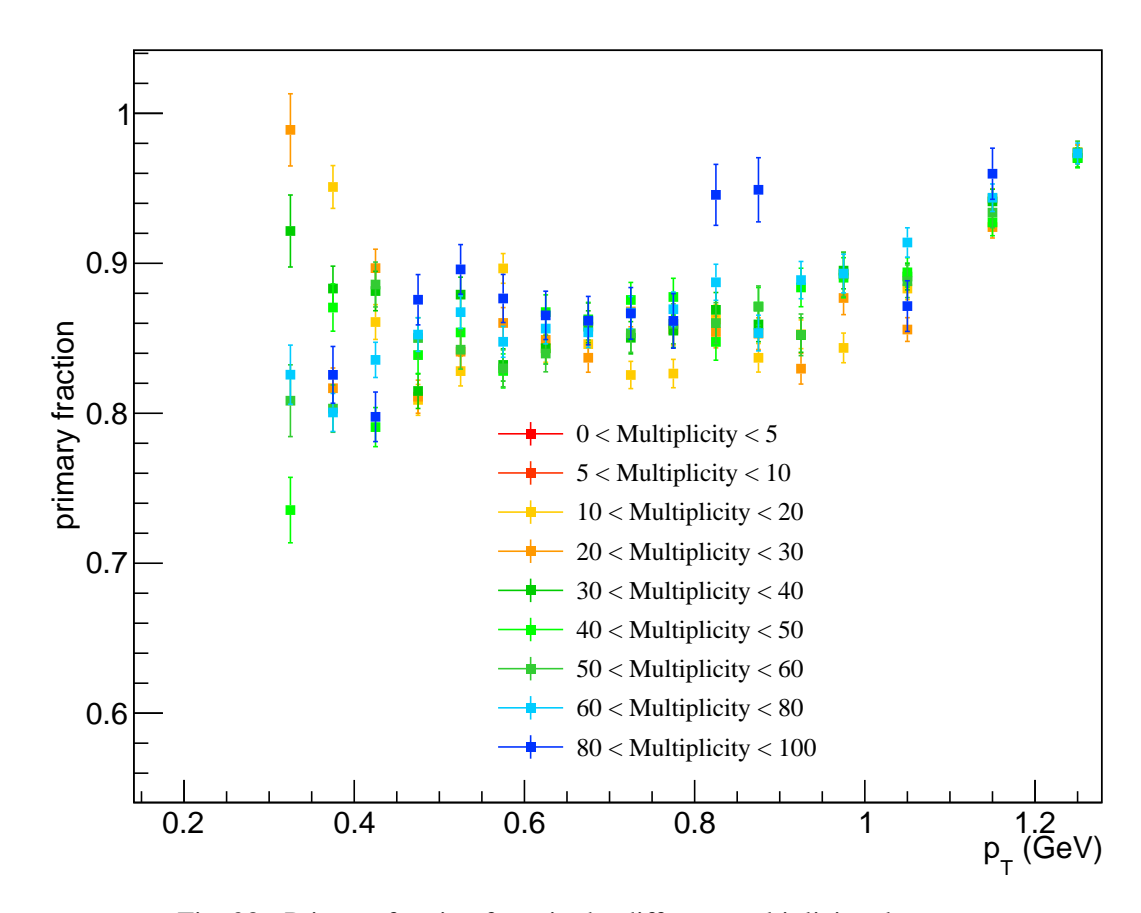


Fig. 38: Primary fraction for  $\bar{p}$  in the different multiplicity classes.

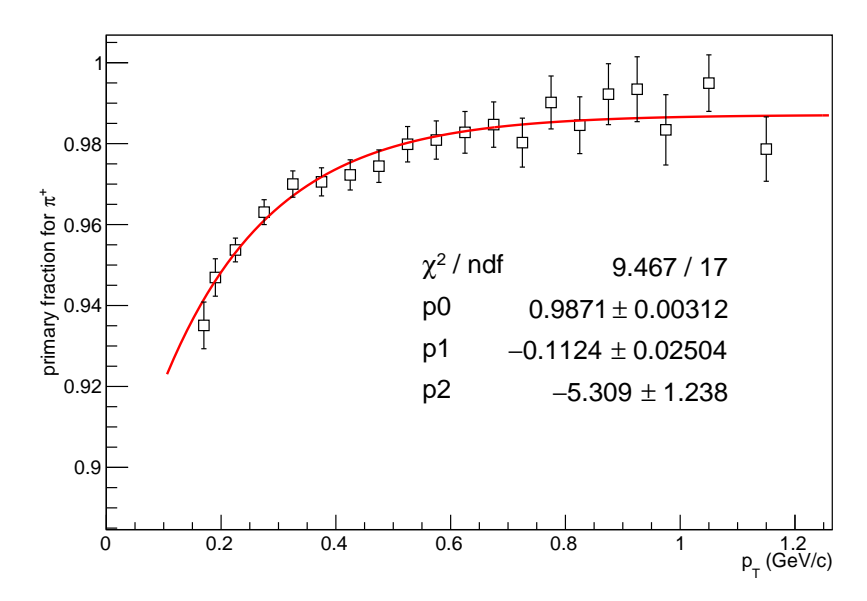


Fig. 39: Example fit to the primary fraction distribution vs.  $p_T$  for positive pions.

### 3. Efficiency on different MC.

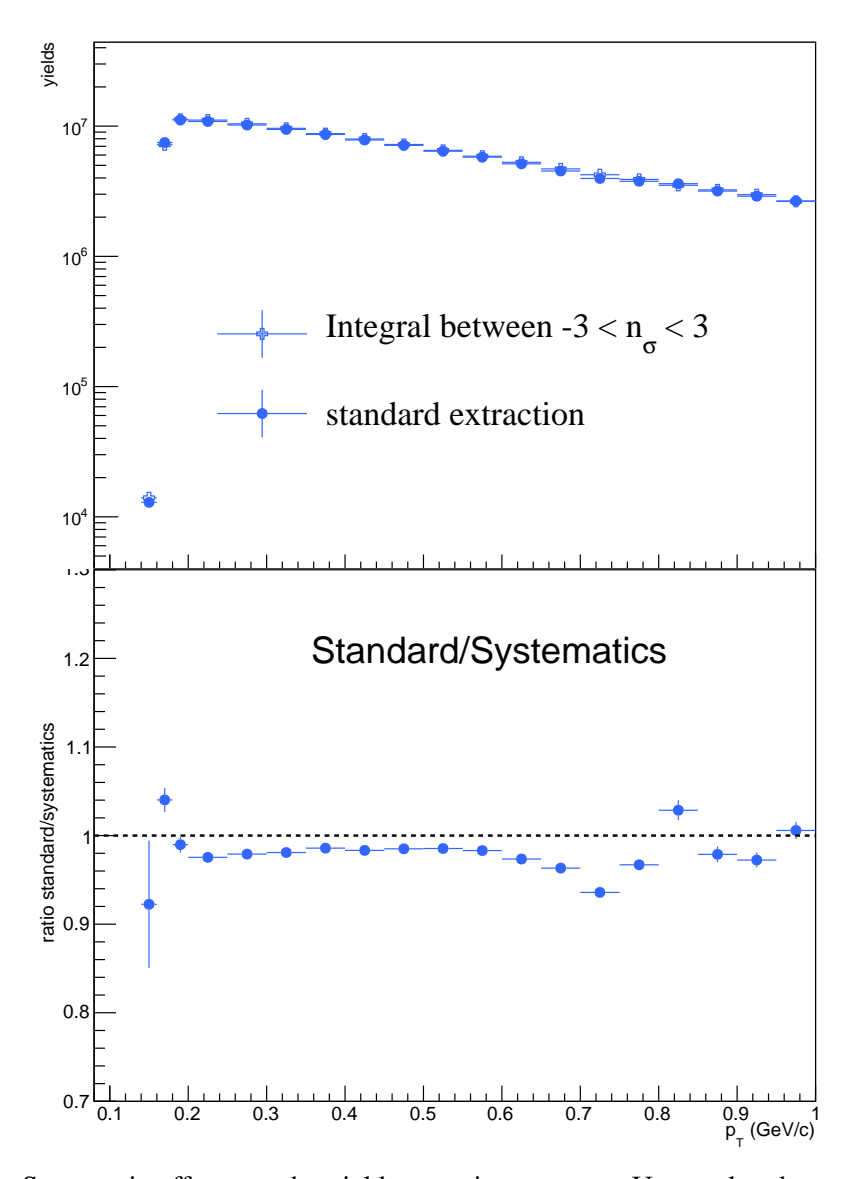


Fig. 40: Systematic effects on the yield extraction strategy. Upper plot shows the spectra for positive pions in multiplicity bin 3 extracted with the default method (fit to  $N_{\sigma}$ ) and with the alternative bin counting approach. Bottom plot shows the ratio among the two. The alternative method is systematically lower since there is no an actual signal unfolding as it happens in the standard approach based on the fit. The overall effect is of a few percent.

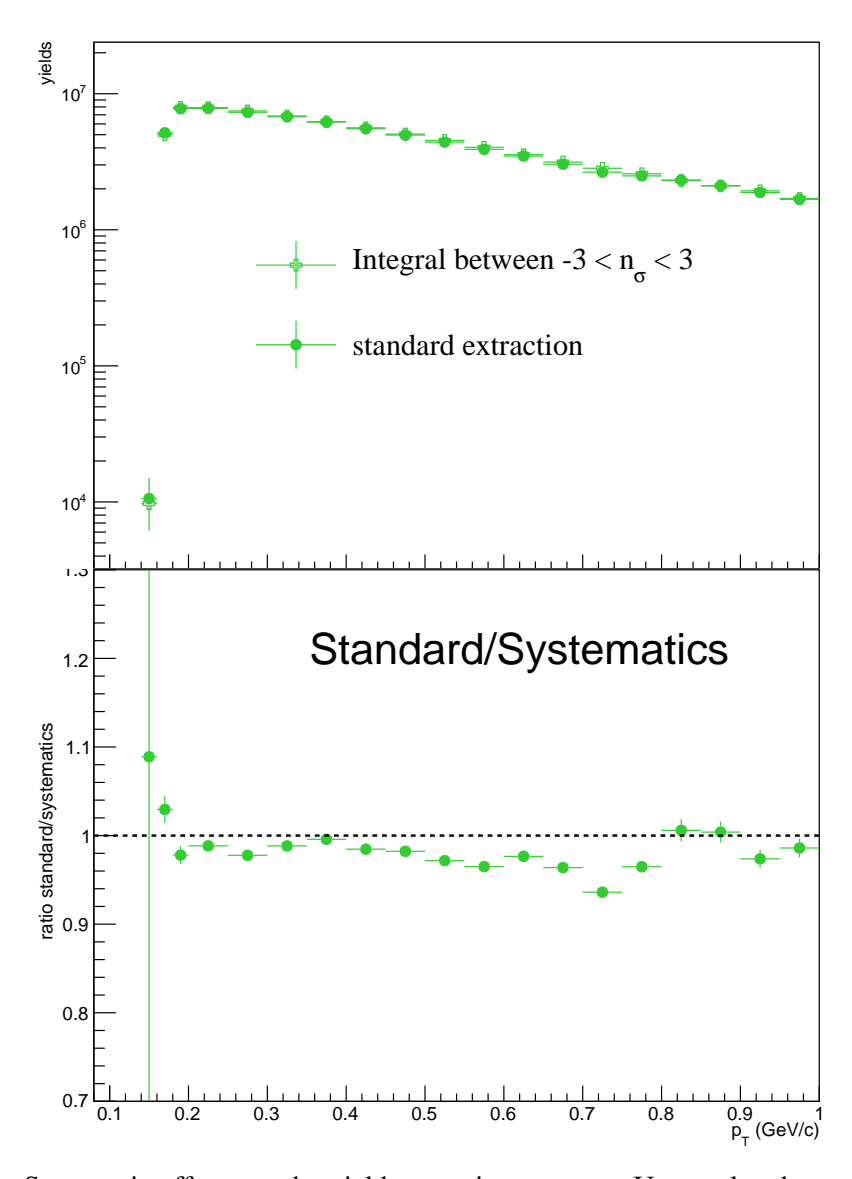


Fig. 41: Systematic effects on the yield extraction strategy. Upper plot shows the spectra for negative pions in multiplicity bin 5 extracted with the default method (fit to  $N_{\sigma}$ ) and with the alternative bin counting approach. Bottom plot shows the ratio among the two. The alternative method is systematically lower since there is no an actual signal unfolding as it happens in the standard approach based on the fit. The overall effect is of a few percent.

#### 5 TOF

In this section, the procedure adopted to select tracks and yields through the particle identification based exclusively on the Time-Of-Flight system is described. The main goal of this analysis is to extract particle yields in the intermediate  $p_T$  region, and match the spectra to the ones extracted in the low- $p_T$  part through ITSsa and TPC. TOF provides PID in the intermediate momentum range, up to 2.5 GeV/c for pions and kaons, and up to 4 GeV/c for protons. The following analysis refers mainly to the analysis notes ALICE-ANA-2013-60 and ALICE-ANA-2017-3545.

#### 5.1 TOF track requirements

This analysis shares with the TPC one (see Sec. 4) the track selection strategy, based on the method AliESDtrackCuts::GetStandardITSTPCTrackCuts2015PbPb( kTRUE, 1 ) illustrated in Sec. 4.1. Furthermore only the global tracks reconstructed through the TPC that match a TOF cluster and for which the arrival time is properly measured, are selected for the TOF sample. These two additional conditions are applied to select good TOF tracks from the TPC sample using the following two methods:

AliESDtrack::kTOFout

AliESDtrack::kTIME

with the first one corresponding to the request of a good TOF cluster match and the second one to the request to have a time correctly assigned. A correct time measurement in TOF detector  $t_{TOF}$  together with the event time  $t_0$  allows to assign a time-of-flight value to the track and so to identify different particle populations, as explained in the next paragraph. The selected TOF sample can be seen in Fig.42 where the particles' beta is shown as a function of the momentum p measured by the TPC.

#### 5.2 PID with TOF detector and signal extraction

The particle identification in TOF standalone analysis follows a statistical approach based on the measurement of the Time-of-Flight *t* for each track matched to the TOF detector:

$$t = t_{TOF} - t_0 \tag{10}$$

For each mass hypothesis the expected Time-of-Flight ( $t_{exp}$ ) can be computed from the track length and the momentum measured in the TPC. So for each mass hypothesis taken in consideration ( $\pi$ , K and p) the distributions of the quantity:

$$t - t_{exp,i} \tag{11}$$

are built for different  $p_t$  bins, selecting tracks in the interval  $0 < y_{CMS}^i < 0.5$ , where  $y_{CMS}^i$  is the rapidity for the mass hypothesis i, as shown e.g. in Fig.43 taking pions as hypothesis The peak

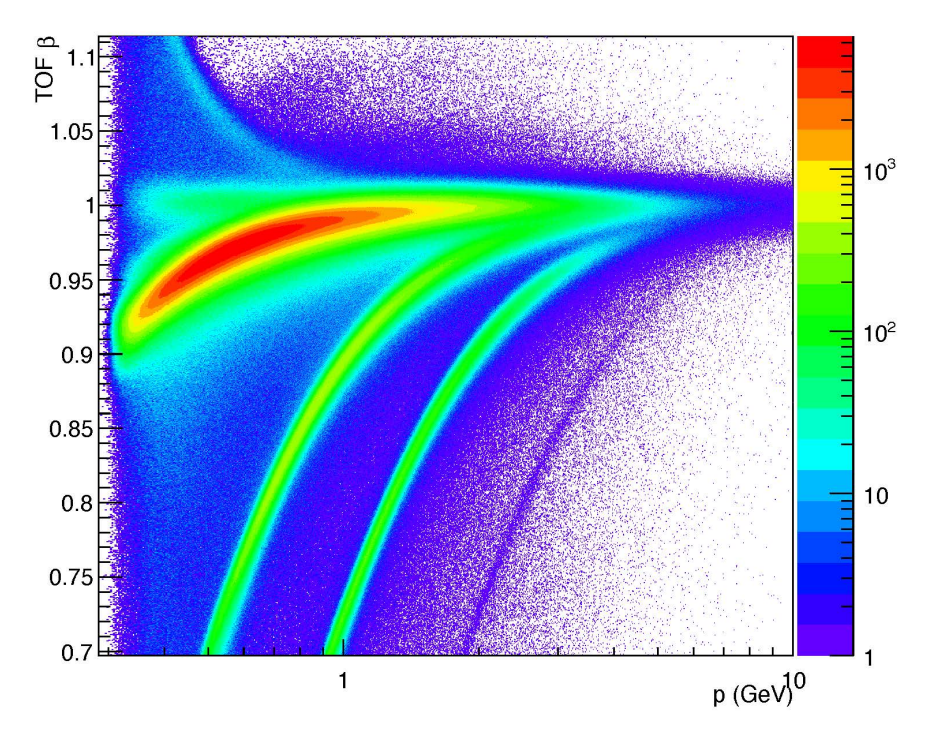


Fig. 42: Beta measured with the TOF detector as a function of the track momentum. The visible bands are from  $e, \mu, \pi, K, p$  and d. The background, outside the bands, is due to tracks that are incorrectly matched to TOF hits in high-multiplicity pPb collisions.

# TOF MB NegPi in pt bin 15 [0.65,0.70] $\boldsymbol{p}_{_{\mathrm{T}}}$

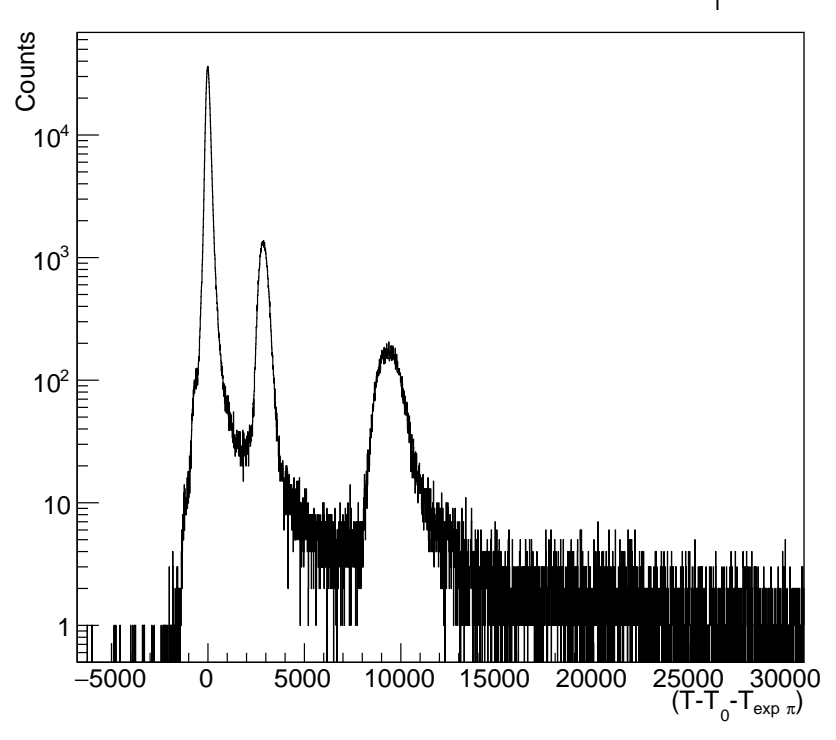


Fig. 43: Distribution of  $t - t_0 - t_{exp,\pi}$ 



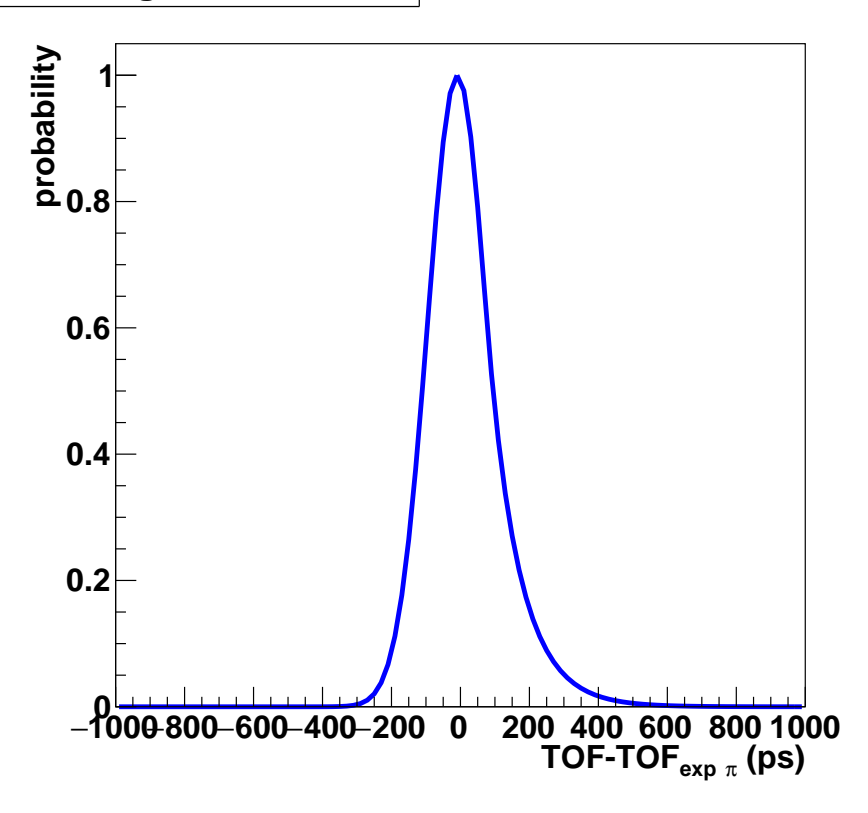


Fig. 44: Distribution of  $t - t_0 - t_{exp,\pi}$ , in the pt bin [0.95, 1]GeV/c

centered in zero corresponds to the pion contribution (in this case the signal related to the mass hypothesis  $i = \pi$ ). The other two peaks are the kaon and proton contamination, respectively, that constitute background of particles j = K, p for the hypothesis  $i = \pi$ . The continuous background under the pion peak that extends also under the kaon and proton peaks is the background contribution due to global tracks associated with a wrong TOF hit, so called mismatch background m. For each contribution a template is built, with a data-driven approach, in order to finally fit the distribution and extract the yields relative to the hypothesis under study, as explained in the following. Each peak is centered in  $t - t_{exp,i} + t_{exp,j}$  and has a spread due to three contributions:

$$\sigma_i^2 = \sigma_{TOF}^2 + \sigma_{t_0}^2 + \sigma_{tracking,i}^2 \tag{12}$$

where  $\sigma_{TOF}$  is the overall TOF detector resolution,  $\sigma_{t_0}$  is the uncertainty on the  $t_0$  measurement and  $\sigma_{tracking,i}$  is the uncertainty on the expected particle Time-of-Flight  $t_{exp,i}$ . In order to extract such  $\sigma_i$  and build the template, the TOF signal has been parametrized using a gaussian with an exponential tail on the right. The parameters used to describe the TOF signal are extracted with a fit to the distribution of  $t - t_{exp,\pi} - t_0$  in the pt bin [0.95, 1]GeV/c, a region where the peak for  $\pi$  is clearly separated in TOF. The function extracted, shown in Fig.44, can describe correctly all the peaks in Fig.43 if an extra smearing (with respect to the  $\sigma_{fit} = 85ps$  obtained in the fit) due

to the tracking is considered. Such smearing take care of the fact that  $\sigma_{exp,i}$  is strongly dependent on pt. Such smearing can be added to the template sampling a gaussian centered in zero with sigma:

$$\sigma_{smearing,i} = \sqrt{\sigma_{exp,i}^2 - \sigma_{fit}^2}$$
 (13)

The final templates are built for each  $p_t$  bin in following way:

$$t_{template,i,j} = t_{exp,j} + t_{exp,i} + TOF signal + ExtraSmearing$$
 (14)

The template m for the mismatch background has been extracted using the method AliTOFPIDResponse::GetMismatchRandomValue(eta) and has been got subtracting the expected Time-of-Flight of the hypothesis specie:

$$m_i = m - t_{exp,i} \tag{15}$$

Fig.45 shows an example of the distribution for tracks with  $0.9 < p_t < 0.95 \ GeV/c$  in 0-5% central pPb collisions under the pion hypotesys i =  $\pi$  together with the expected signal distribution, the expected particle-background distribution of kaons and protons j=K,p and the expected mismatch-background distribution ( $m_{\pi}$ ). The expected contributions are shown with the normalization factor obtained from the global fit to the data, performed with the *RooFit* utility.

#### 5.3 Primary fraction

Following the same procedure described for TPC (see Sec. 4.5.4), primary fractions have been extracted for TOF too. Differently from the TPC case, in order to select a proper set of tracks with the desired identity on data a cut on the combined  $N_{\sigma}$  from TPC and TOF is adopted. Namely, the cut

$$N_{\sigma^{TPC-TOF}} < 2$$
 (16)

is adopted for any particle species, where

$$\sigma^{TPC-TOF} = \sqrt{\sigma_{TPC}^2 + \sigma_{TOF}^2}.$$
 (17)

In this way, a proper sample of particles *i* is obtained from data, and the template distributions obtained from MC are scaled and fitted to them in order to get the primary fractions. As an example of the fit performances, in Figs. 46 and 47 the fit for pions and protons are shown, respectively.

In Fig.47 the fit has been done with the *TFractionFitter* utility, while in Fig.46 the fit has been done with the *RooFit* utility. The primary corrections, shown in Fig.48 for protons and in Fig. 49 for pions, have been obtained for each  $p_t$  bin using both the fitting utility: *TFractionFitter* has been taken as default result and the one obtained with *RooFit* as systematic of the fitting procedure. As can be seen such systematics is less than 0.6%.

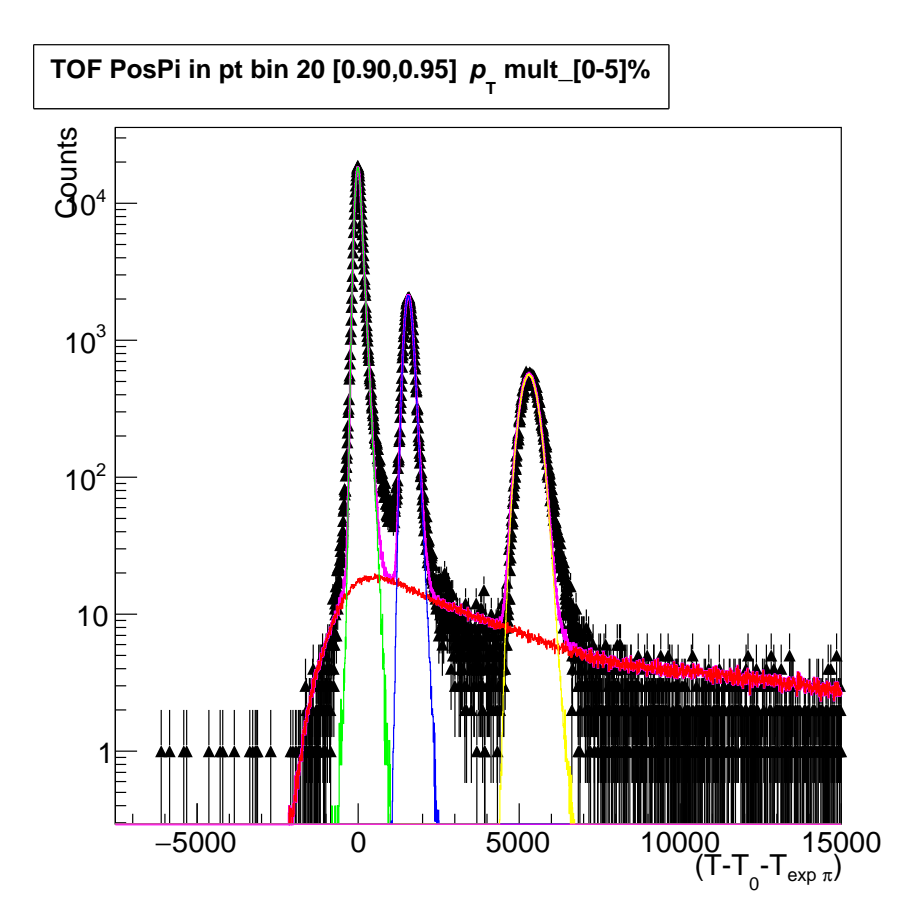


Fig. 45: Distribution of  $t - t_0 - t_{exp,\pi}$  fitted with the built templates

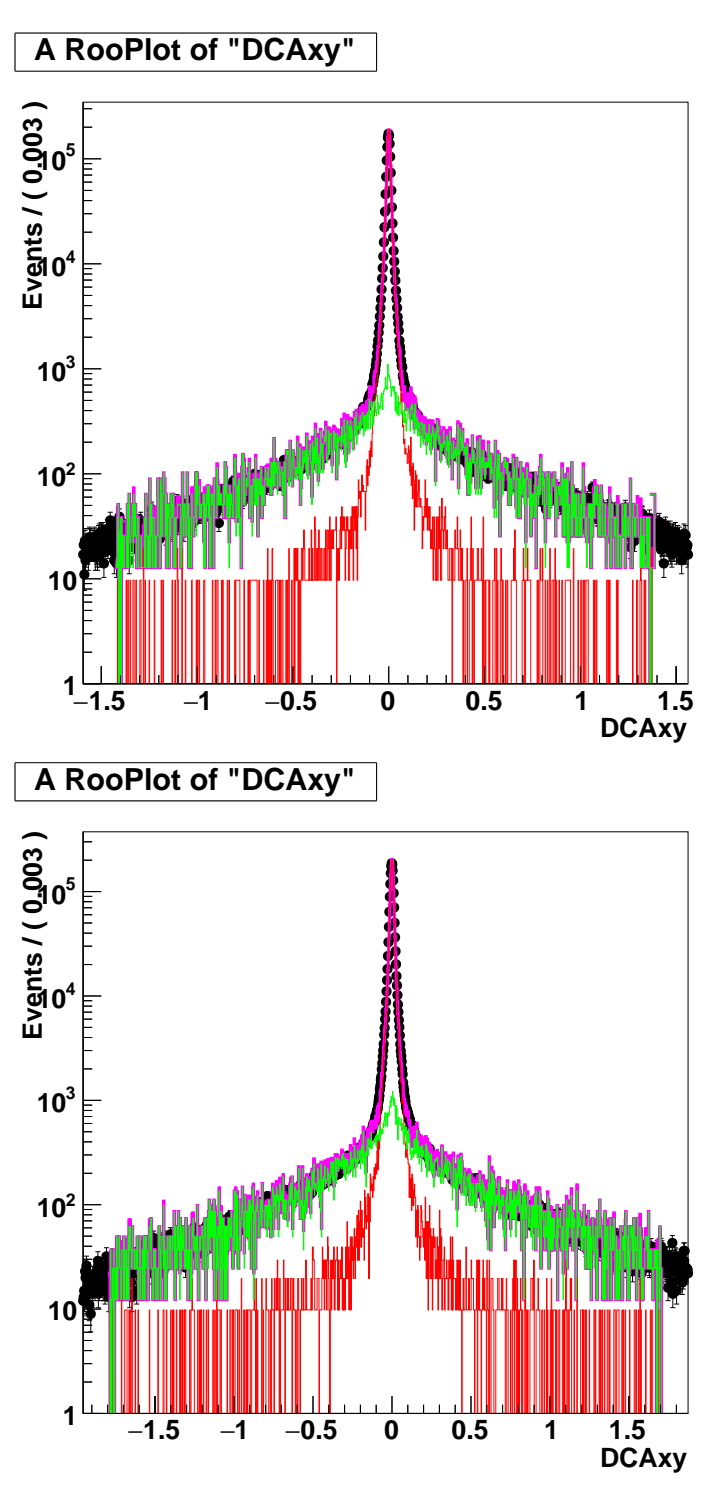


Fig. 46: Fit to DCA distribution in two  $p_T$  bins for positive (top) and negative (bottom) protons identified through the TOF system. The fit is performed through RooFit.

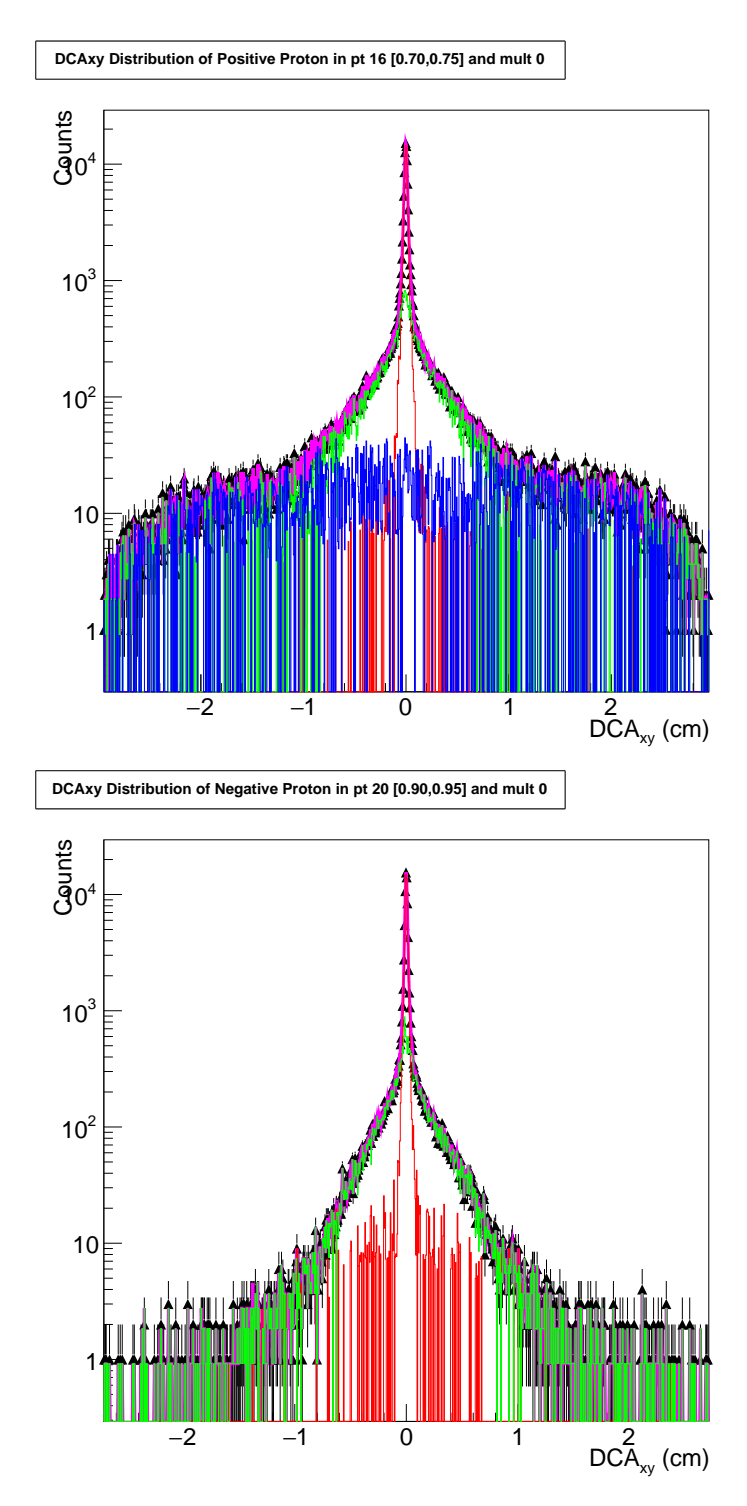


Fig. 47: Fit to DCA distribution in two  $p_T$  bins for positive (top) and negative (bottom) protons identified through the TOF system. The fit is performed through TFractionFitter.

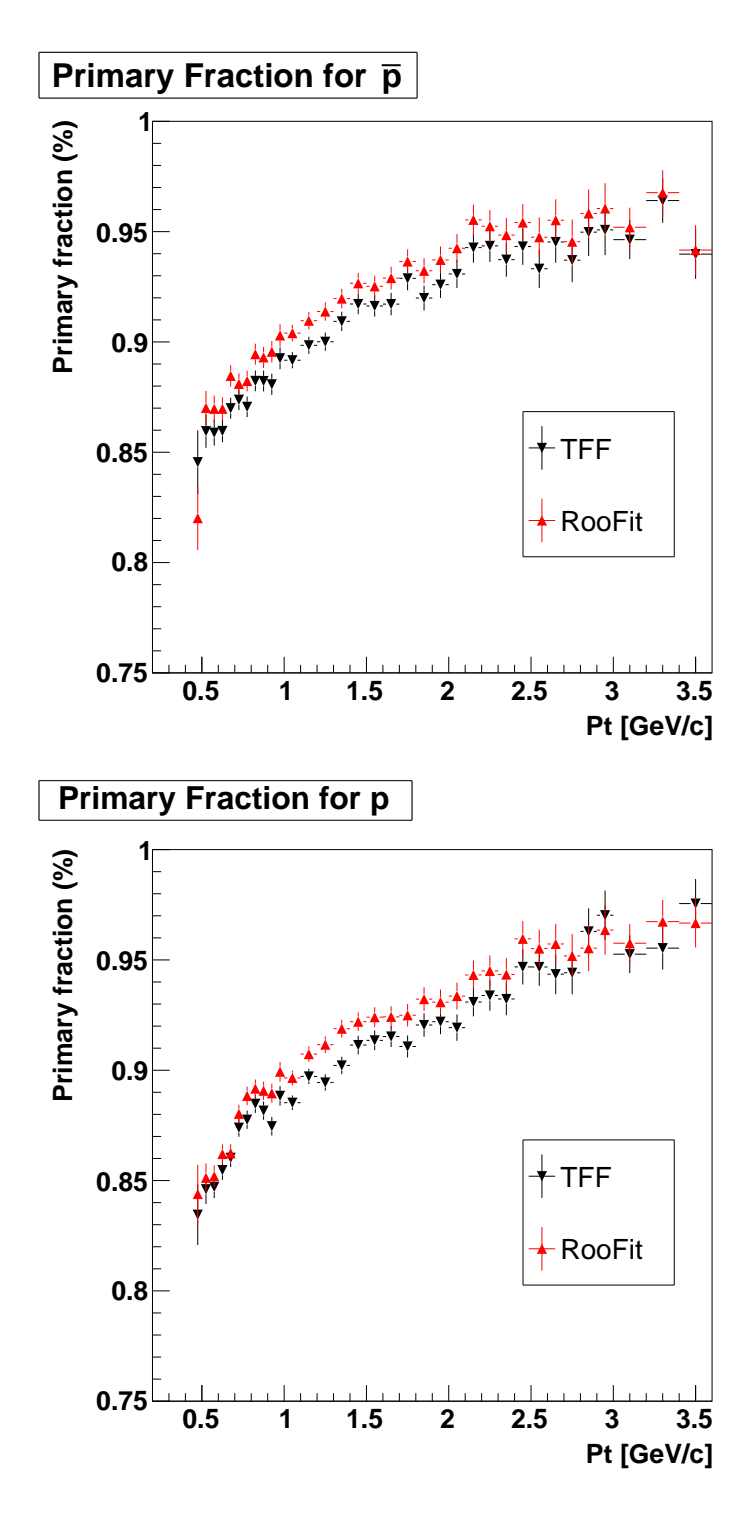


Fig. 48: Comparison of primary fraction corrections using RooFit and TFractionFitter fit utilities for protons.

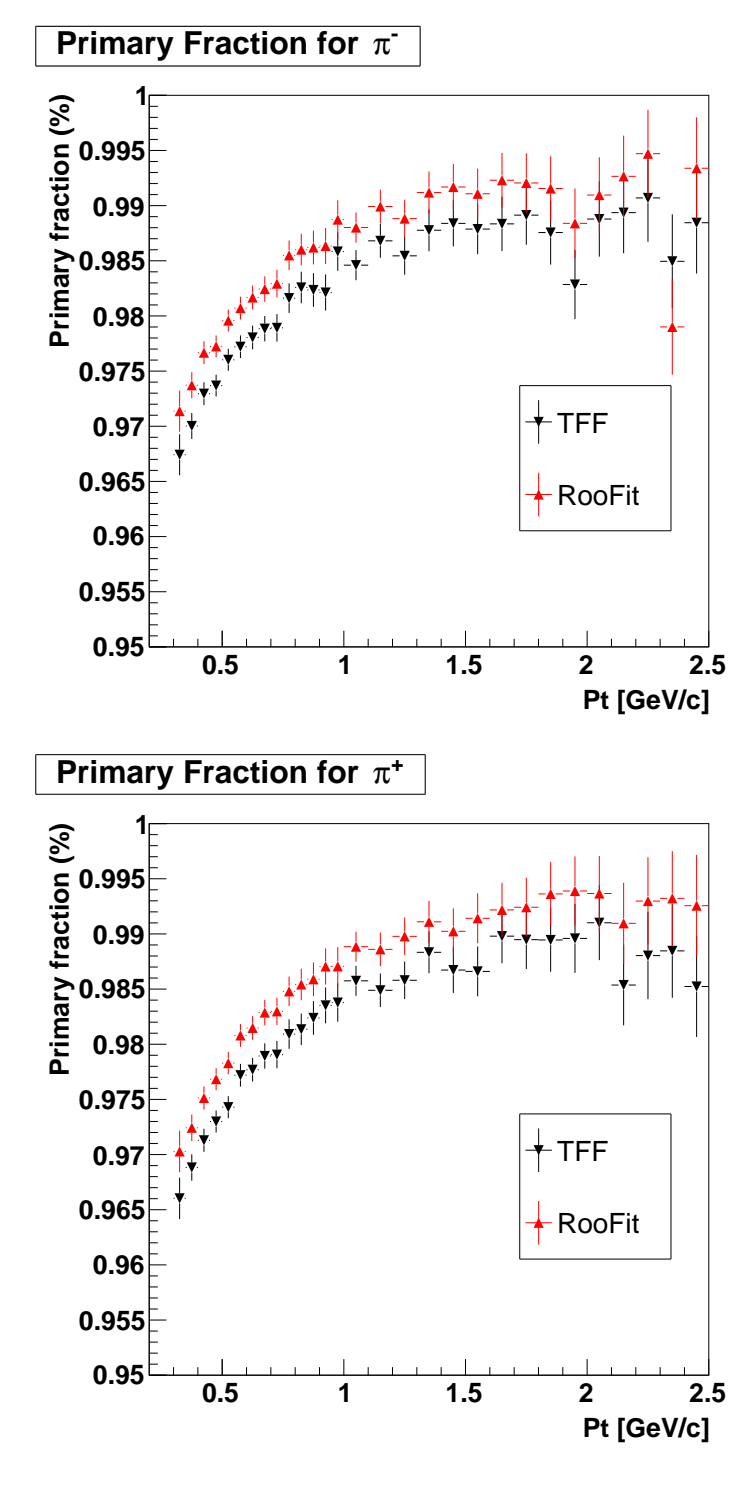


Fig. 49: Comparison of primary fraction corrections using RooFit and TFractionFitter fit utilities for pions.

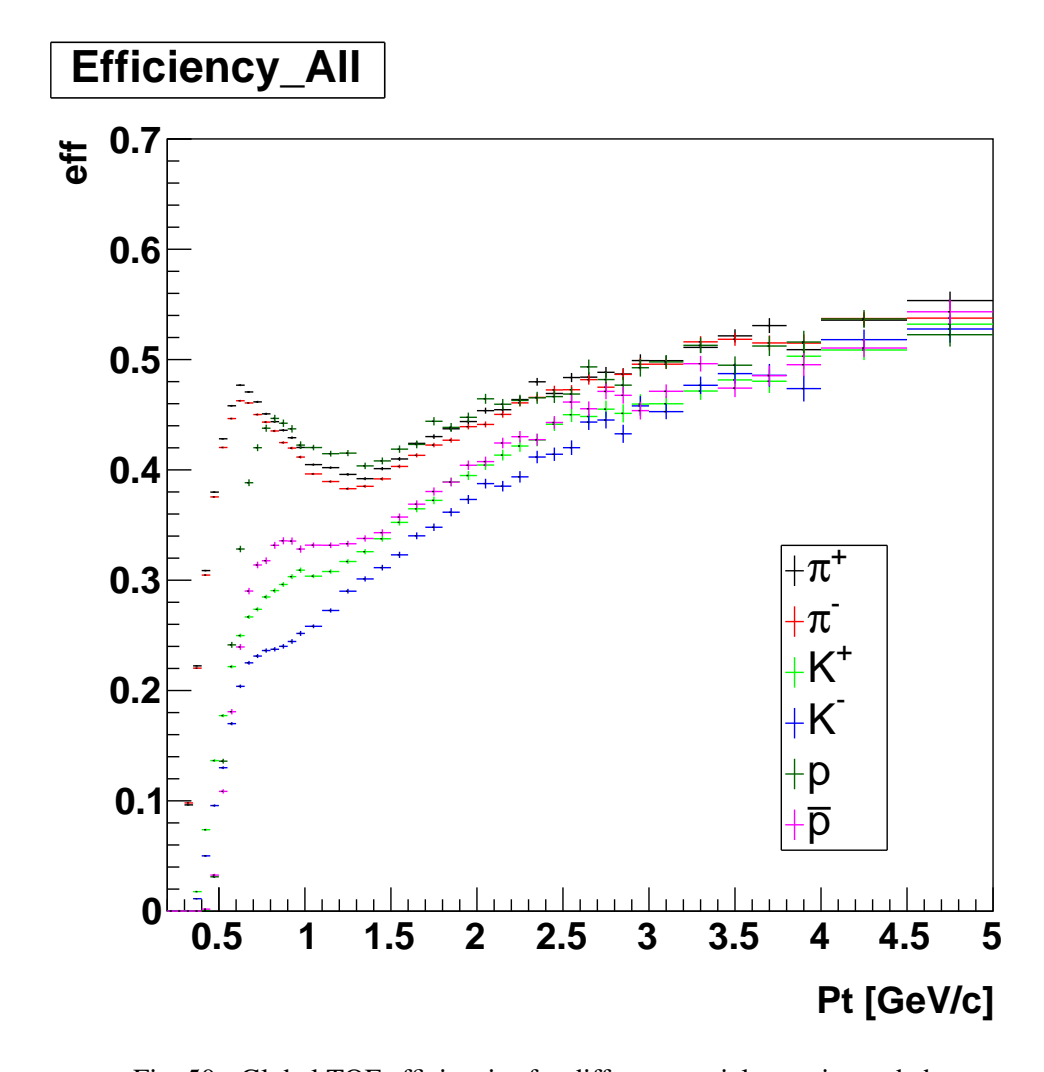


Fig. 50: Global TOF efficiencies for different particle species and charges.

#### 5.4 Efficiency correction

For TOF, a global efficiency is introduced, representing the product between the tracking efficiency previously introduced (see Sec. 4.5.1) and the matching efficiency specific for the TOF system, that take care of the number of matched tracks with TOF with respect to the global tracks reconstructed by the TPC. In Fig. 50 the TOF efficiency for the different particles are shown, while Figs. from 51 to 56 show the efficiencies for the separated particles in the different multiplicity classes.

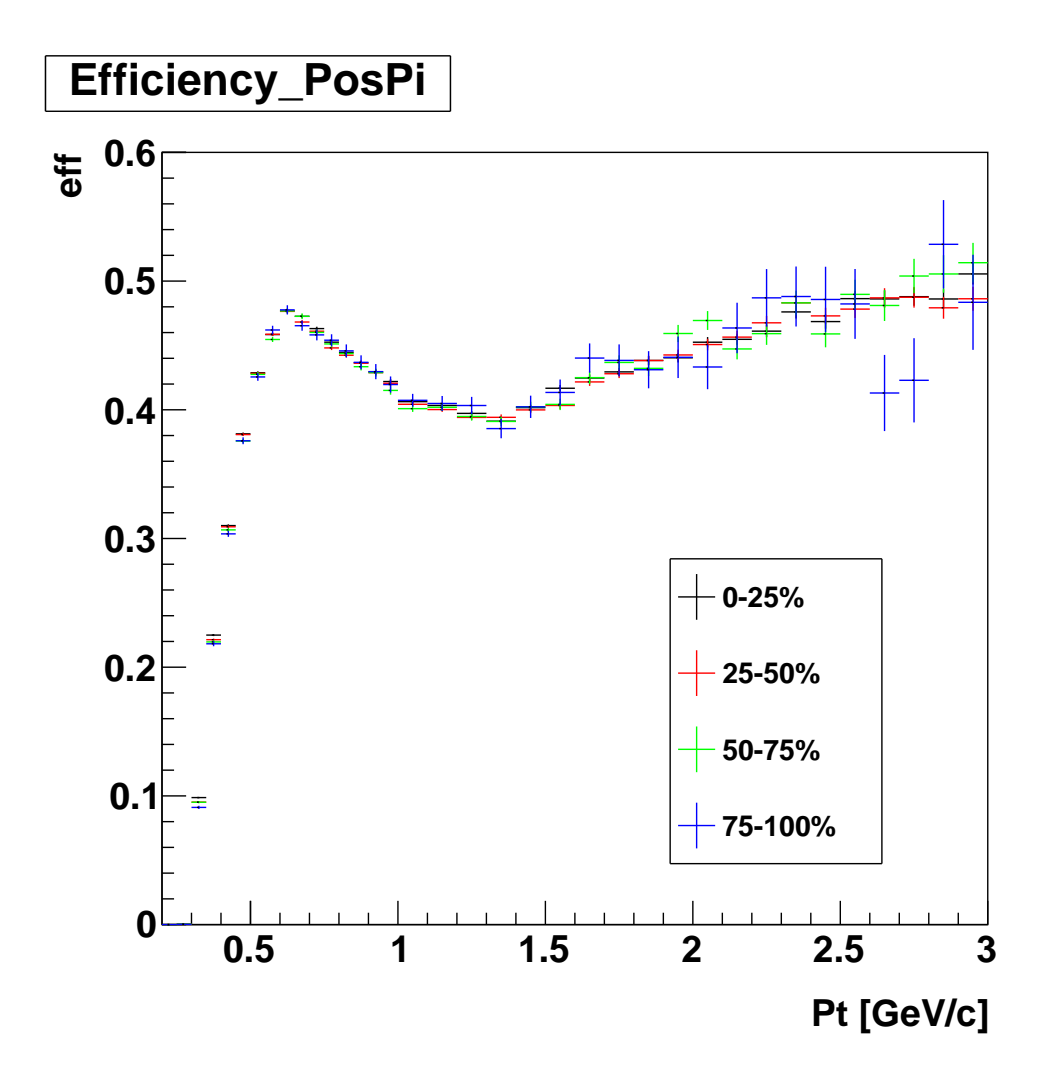


Fig. 51: Global TOF efficiencies for positive pions in four different multiplicity classes.

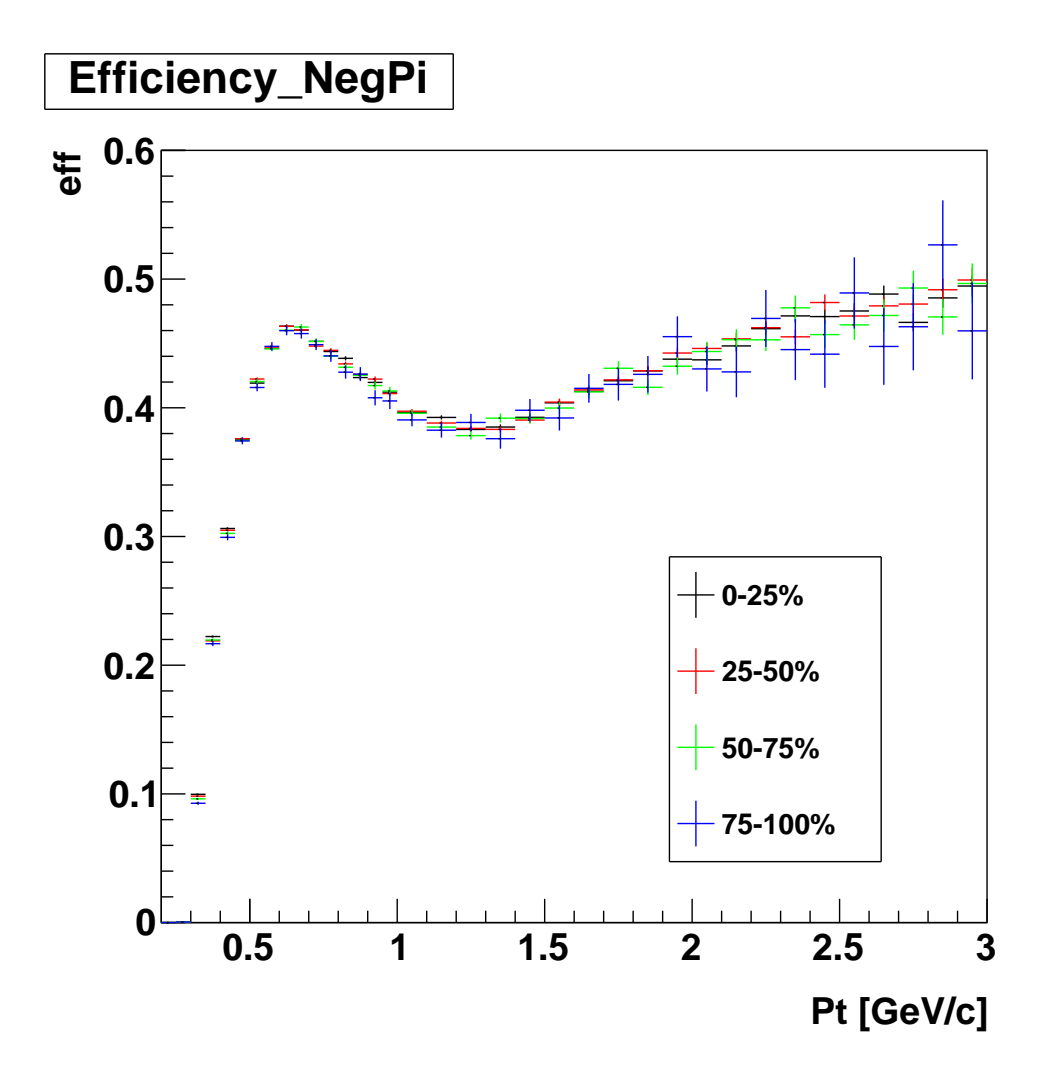


Fig. 52: Global TOF efficiencies for negative pions in four different multiplicity classes.

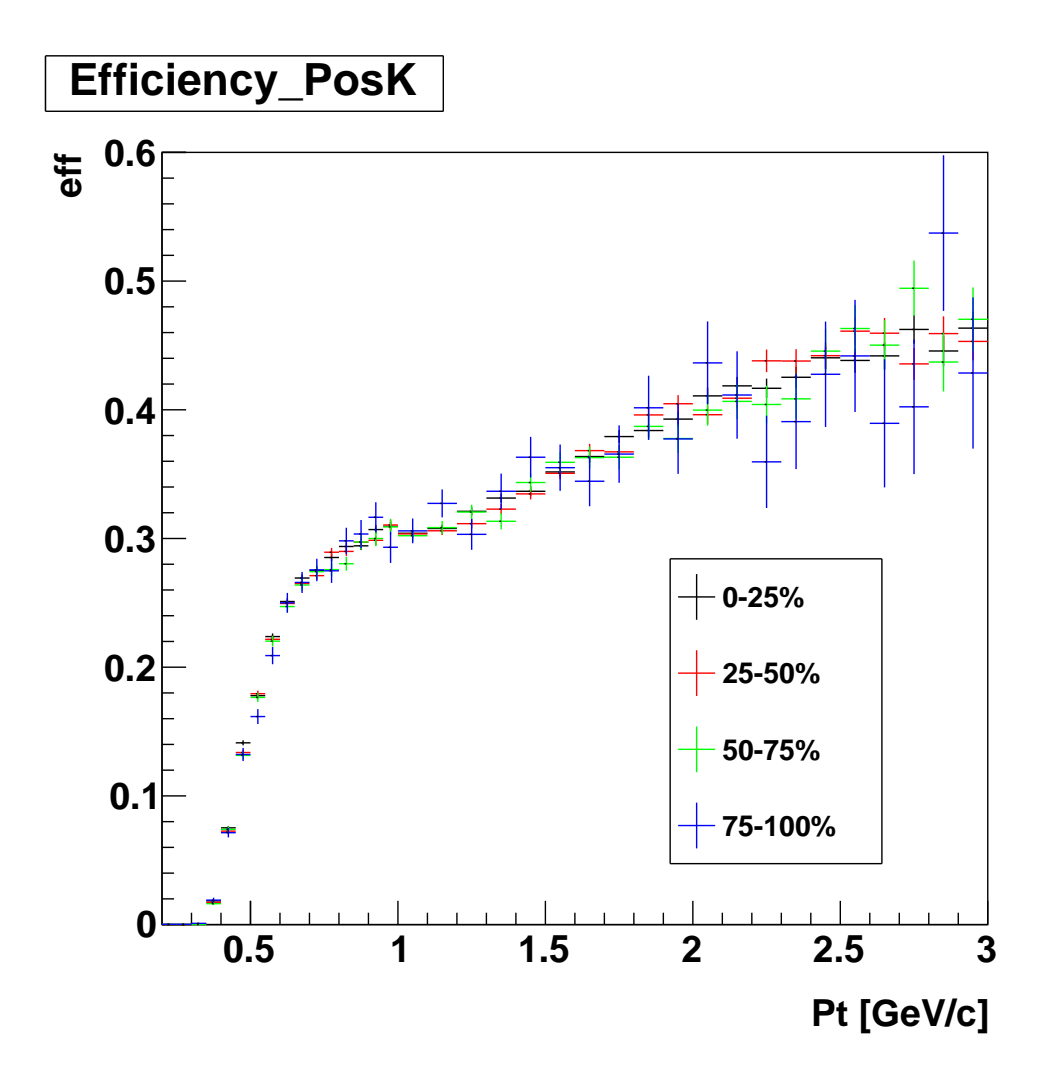


Fig. 53: Global TOF efficiencies for positive kaons in four different multiplicity classes.

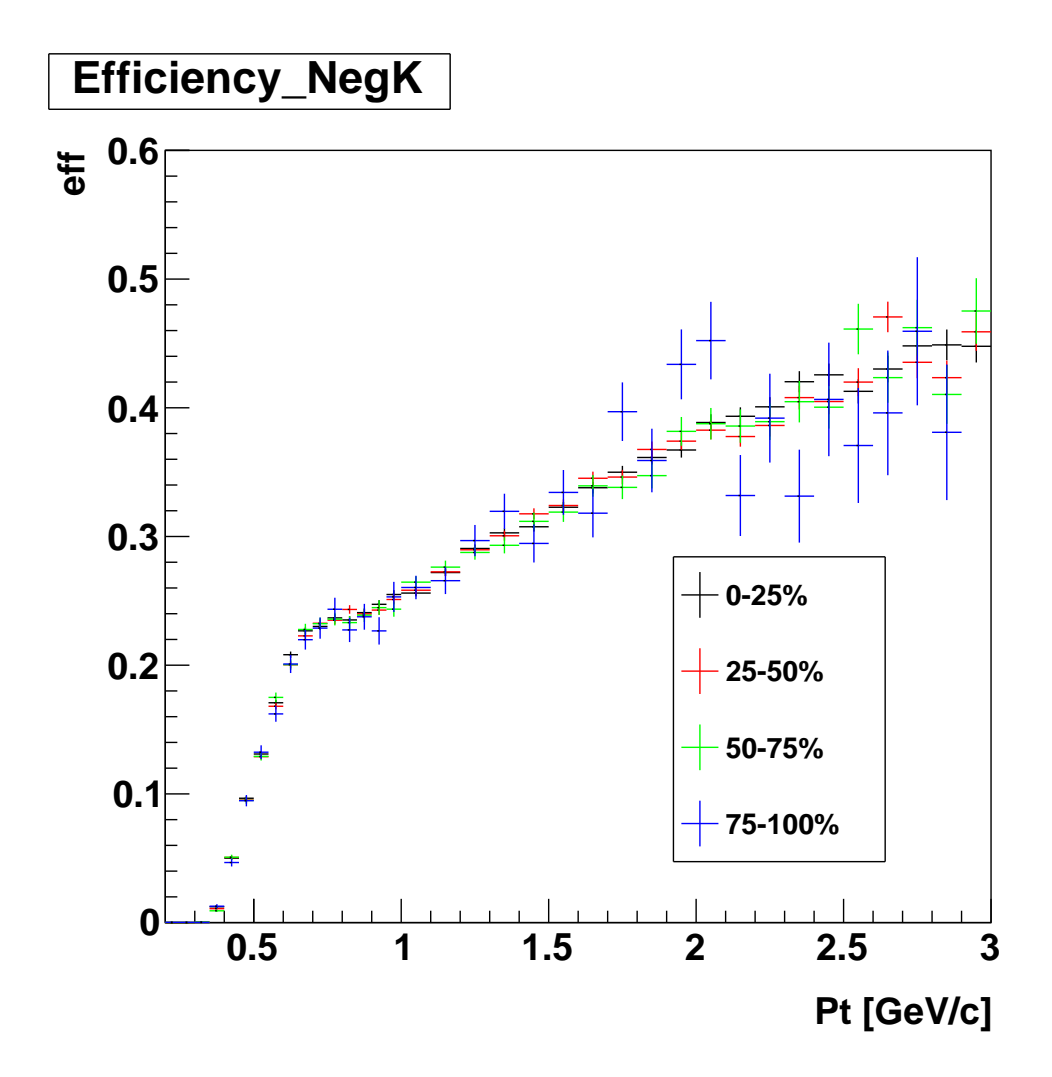


Fig. 54: Global TOF efficiencies for negative kaons in four different multiplicity classes.

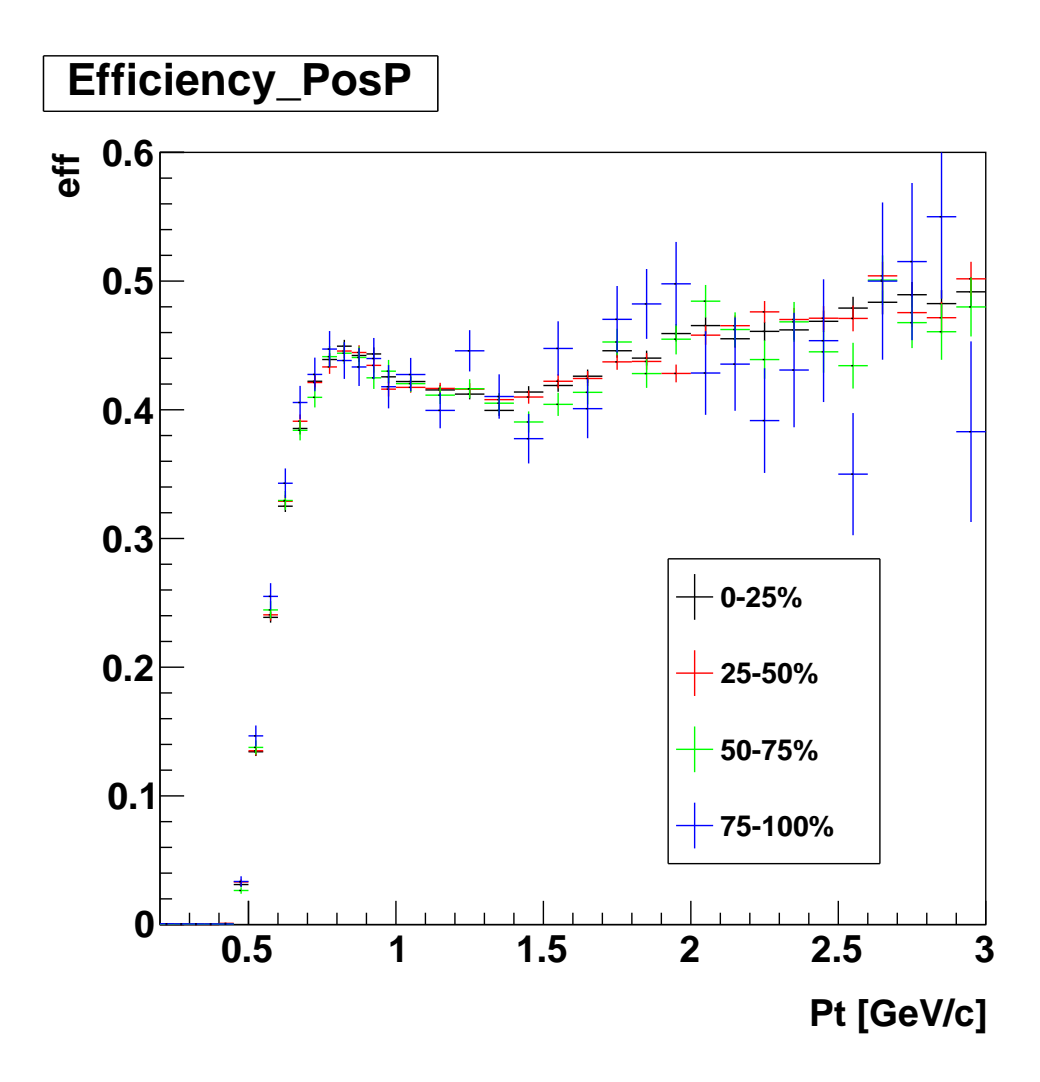


Fig. 55: Global TOF efficiencies for positive protons in four different multiplicity classes.

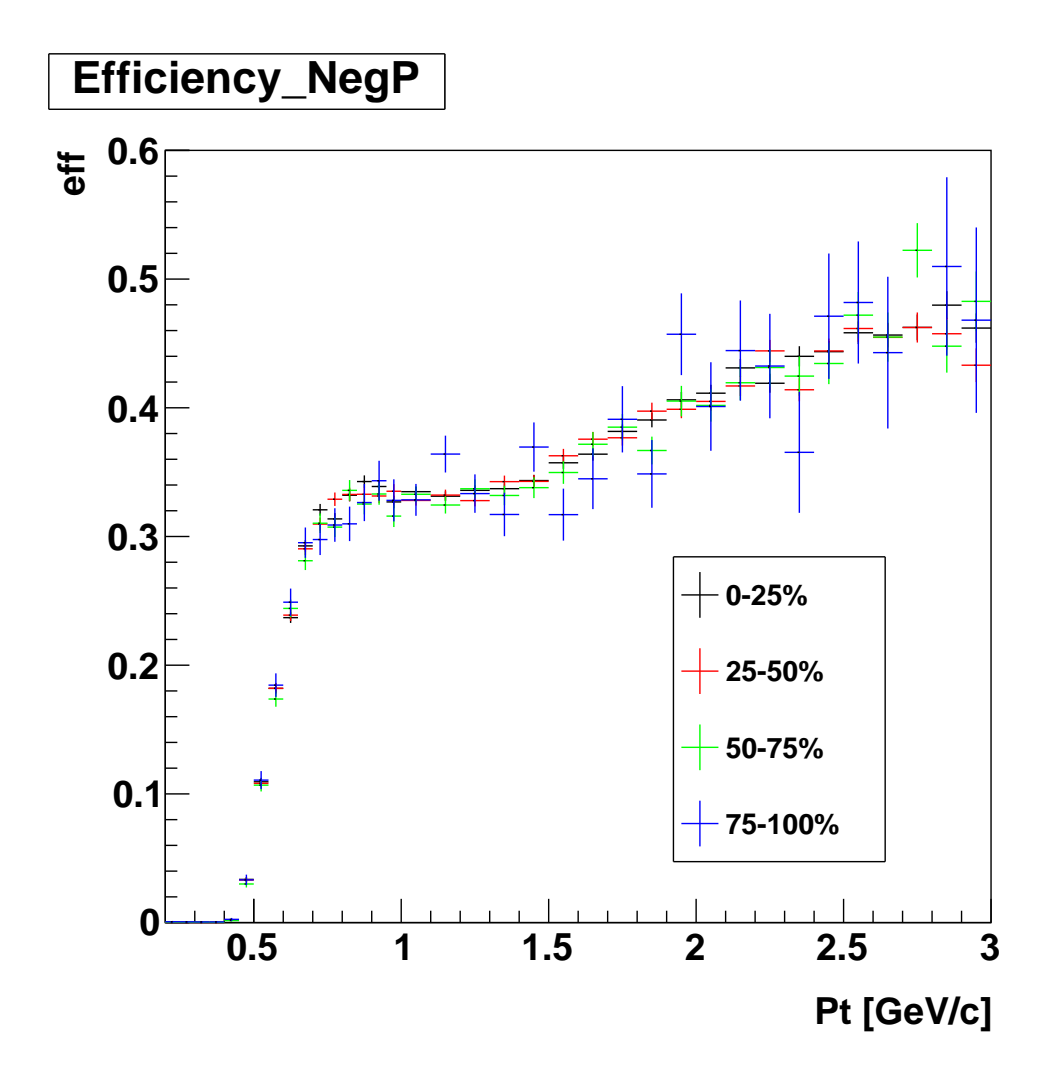


Fig. 56: Global TOF efficiencies for antiprotons in four different multiplicity classes.

## Combined Results